The Linnean Society of London
ZOOLOGICAL Journal of the Linnean Society

Reappraisal and new material of the holotype of *Draconyx loureiroi* (Ornithischia: Iguanodontia) provide insights on the *tempo* and *modo* of evolution of thumb-spiked dinosaurs

Journal:	*Zoological Journal of the Linnean Society*
Manuscript ID	ZOJ-04-2021-4539.R1
Manuscript Type:	Original Article
Keywords:	phylogenetic systematics < Phylogenetics, Jurassic < Palaeontology, Cretaceous < Palaeontology, Evolution, evolutionary rates < Evolution, Dinosauria < Taxa, Bayesian inference < Phylogenetics, Europe < Geography

Abstract:	Upper Jurassic Lourinhã Formation is notorious worldwide for its rich assemblage of fossil vertebrates. Ornithopod dinosaurs are represented by two iguanodontian species *Eousdryosaurus nanohallucis* and *Draconyx loureiroi*. Recently, we were made aware of unreported material belonging to the holotype *Draconyx loureiroi*, constituted by partially articulated manual elements. We here redescribe the holotype specimen ML 357, including the new material. The specimen was subjected to CT-scanning and its surface data used to assess anatomical characters. Linear measurements of metatarsal III was used to estimate the body length of the specimen. *D. loureiroi* holotype was included in two different dataset and analysed both with Maximum Parsimony approaches and both with Bayesian inference to estimate evolutionary rates across the base of Iguanodontia. We present evidence that *Draconyx loureiroi* is a valid taxon, nested within Styracosterna and clearly diagnosable by a unique combination of characters. Both Maximum Parsimony and Bayesian inference indicate high evolutionary rates across Jurassic/Cretaceous transition for the base of Iguanodontia. Length estimation suggests that *Draconyx loureiroi* was a relatively small, bipedal and possibly cursorial animal. Given its basal phyletic position we interpret this bauplan was the ancestral condition for Styracosterna, that only later in the Cretaceous evolved into giant quadrupedal forms.

Introduction

Iguanodontia (*sensu* Madzia *et al*., 2018) is a highly diverse ~~speciose~~ clade of ornithischian dinosaurs with basal forms (non-hadrosauroid) being a usual component of Late Jurassic and Early Cretaceous ecosystems (Galton, 1980a, 2006, 2009; McDonald *et al*., 2010; Foster, 2020). Despite their very long history of research ~~(Owen, 1842)~~(Mantell, 1925), and their widespread biogeographic distribution, most of what is known regarding the anatomy and phyletic relationships of Late Jurassic species is relegated to the North American continent, and Africa. On the other hand, Europe has produced many relevant specimens and species dated to the Early Cretaceous (Norman, 1980, 1986, 2004, 2015; McDonald *et al*., 2012), while Late Jurassic taxa are represented by fewer and in some cases very incomplete specimens (Galton & Powell, 1980; Mateus & Antunes, 2001; Ruiz-Omeñaca *et al*., 2006, Escaso *et al*., 2014).

The relationships at the base of Iguanodontia (and ~~-~~more generally in basal ~~more in general~~, Ornithopoda) have undergone several changes in recent years (Boyd, 2015; Dieudonné *et al*., 2016, 2020; Madzia *et al*., 2018; Bell *et al*., 2018; Herne *et al*., 2019; Rozadilla *et al*., 2019), profiling a more complex evolutionary history of this clade than previously inferred ~~by previous analyses of~~(e.g. ~~-~~McDonald ~~(~~, 2012~~,) and ~~Norman; ~~(2015~~))~~. After McDonald (2012) and derived matrices (Xu *et al*., 2018; Verdú *et al*. 2018, 2019) ~~a handful of~~several studies have considered the global relationships of Iguanodontia, often focusing on less inclusive clades (Boyd, 2015; Madzia *et al*., 2018; Dieudonné *et al*., 2020). European taxa, despite their paucity and poor-preservation, may help to untangl~~eing~~ the intricate evolutionary scenario at the root of Iguanodontia. Recently, two independent lines of evidence (ichnological and body fossil records) have pointed out that diversity of iguanodontians in the Late Jurassic of Europe may have been underestimated, suggesting the

presence of styracosternans more similar to Early Cretaceous forms than to other coeval iguanodontians (Castanera *et al*., 2020a,b; Rotatori *et al*., 2020).

Draconyx loureiroi is one of the two ornithopod taxa described from the Late Jurassic of the Iberian Peninsula. The holotype ML 357 and the only specimen so far, is a medium-sized iguanodontian that was recovered from ~~in~~ the Upper Jurassic Lourinhã Formation (Portugal) in 1991 (Mateus & Antunes, 2001). Histological studies have shown that ML 357 is a senile individual, approximately 30 years old (Waskow & Mateus, 2017). Mateus & Antunes (2001) classified the specimen as a basal iguanodontian, attributing the species to the family 'Camptosauridae', composed at that time ~~by~~ of the species *Camptosaurus dispar*, '*Camptosaurus' prestwichii*, *Callovosaurus leedsi* and *Draconyx loureiroi*. ~~Following~~ Subsequent analyses by McDonald (2011) recovered the genus *Camptosaurus* as paraphyletic, while Ruiz-Omeñaca *et al*. (2006) have recovered *Callovosaurus leedsi* as a member of Dryosauridae. Since then, the clade 'Camptosauridae' has been recovered from few analyses with very weak support (i.e. Verdù *et al*. 2018). ~~Many~~ Other authors treated *Draconyx loureiroi* either as a wildcard taxon (McDonald, 2012) or they excluded it *a priori* in ~~most of~~ their analyses due to its fragmentary condition. ~~,~~ Recently, Verdù *et al*. (2018) ~~.~~ ~~being~~ recovered ~~usually~~*D. loureiroi* in a more derived position than *Camptosaurus dispar*. ~~by the analysis of Verdù *et al*. (2018).~~

In the present study, we contribute to ~~the~~our knowledge of the anatomy and ~~phyletic~~ phylogenetic relationships of Late Jurassic European ornithopod taxa by~~,~~ re-describing the holotype of *Draconyx loureiroi* (ML 357)~~,~~and including undescribed material that was made available by the original collector ~~recently~~. We analyse in detail its phylogenetic relationships and its significance for the evolutionary history of iguanodontians via time-calibrated analysis employing both Maximum Parsimony and Bayesian inference. The results indicate a

more deeply-~~-~~nested position within Ankylopollexia than previously inferred by other authors.

Abbreviations: ML, Museu da Lourinhã, Lourinhã, Portugal; SHN, Sociedade de História Natural, Torres Vedras, Portugal; NM~~H~~N~~M~~H, National Museum of Natural History~~-~~, Washington DC, U.S.A~~Museum~~.

Geological settings

The Lourinhã Formation (Fig.1) is an heterogenous siliciclastic succession of continental deposits dated to the Kimmeridgian-Tithonian interval and~~,~~ located in the Meso-Cenozoic Lusitanian Basin (Kullberg *et al*., 2014)~~,~~ whose subdivisions have been ~~largely~~ debated (Hill, 1989, Taylor *et al*., 2014). Generally, it is ~~constituted by~~composed of sandstones and mudstones with rare limestone intercalations, representing a braided fluvial system and alluvial fans, with occasional marine transgressions (Hill, 1989; Taylor *et al*., 2014). Since a detailed revision and overview of this lithostratigraphic unit is beyond the scope of the present study, we follow for simplicity the subdivision described by Mateus *et al*. (2017). The Lourinhã Fm. outcrops in two sub-basins: the Consolação ~~basin~~ and Turcifal sub-basins. In the first of these, three ~~M~~members are distinctly recognizable (from bottom to top): Porto Novo/Praia da Amoreira Member, Praia Azul Member and Santa Rita Member. In the Turcifal sub-basin, the only m~~M~~ember outcropping is the Assenta Member, which is laterally equivalent to the Santa Rita Member.

The *Draconyx loureiroi* holotype ~~has been~~was recovered from the Praia Azul Member, which is constituted by three extensive carbonated shell-layers, cutting a succession of fine mudstones (Hill, 1989; Taylor *et al*., 2014). Each layer represents a marine

transgression episode, being the second layer also the transition between the Kimmeridgian and Tithonian stages (Hill, 1989; Taylor *et al*., 2014; Mateus *et al*., 2017). The specimen ~~has been~~was recovered just above the second layer, ~~therefore~~ and is therefore considered lower~~-~~most Tithonian in age (Mateus & Antunes, 2001).

Material and methods

~~The specimen~~ ML 357 is a partial skeleton, including appendicular and axial elements. It was recovered in~~-~~ 1991 and ~~hosted~~ has been housed since then in the ~~its~~ collections ~~by~~of the Museu da Lourinhã. The specimen includes ~~presents~~ an almost complete and articulated foot and several other disarticulated and isolated postcranial elements. We were recently informed by the discoverer of ML357, Carlos Anunciação, of ~~about~~ the existence of unreported material from the holotype specimen, stored in his home since its collection in 1991. This unreported material has been donated to the Museu da Lourinhã, and is included in ML 357 entry number. This material includes manual phalanges and further carpal elements. This material is clearly ~~for~~from the same locality and is ~~coherent~~ consistent with the size and ~~taxonomy~~ other features of ML 357. Furthermore, the lack of repeated elements supports the interpretation that both the old ~~material~~ and the new material~~one~~ represents the same ~~single~~ individual. In addition, the fragments of rock attached to the bones of the new ~~reported~~ material, a dense grey muddy siltstone ~~were~~ are identical to those ~~attached to the one~~ found encasing the old material , ~~thus~~ adding further support to the idea that it is ~~we considered~~ it part of the same individual. Both the old and new material of ML 357 ha~~ves~~ been prepared mechanically, and its post-cranium, except for the manual elements, ~~was then~~has been subjected to CT-~~S~~scanning in order to produce a three dimensional model to illustrate its anatomy and better assess its phylogenetic characters. The specimen was scanned first utilizing the ~~V~~veterinary facility of “Hospital veterinario do Oeste” ~~by the machine~~using a Siemens Somatom Emotion 6 with voltage set to

130kV and a current of 200 µA. To improve the resolution of the first scan, the tarsus and pedal elements were re-scanned by the company "MiconSense" using a ~~with the machine~~ GE VtomeX M 240, with voltage of 200 kV and a current of 500 µA. It was not possible to segment the specimen because of the noise caused by permineralization due to diagenetic processes. Therefore, the surface data were exported as 3D meshes by Avizo v.9 in the free software Blender (Hess, 2010), and anatomical structures were isolated. As a third step, the specimen was articulated and rendered producing the images present herein.

To test its phylogenetic affinities, ~~it~~ ML 357 comprising of both the old and new reported material, was included first into Boyd (2015) dataset, following the modifications of Madzia *et al*. (2018) and Bell *et al*. (2018). We performed just one global analysis, since the new material did not provide any new character score. The analysis was carried out in TNT v.1.5 (Goloboff & Catalano, 2016), the tree search was performed in two steps, as described by Bell et al. (2018): a~~A~~ 'New Technology Search' was carried to find starting trees, setting 30 cycles of Drift and 50 cycles of Ratchet. Default options were used for the other parameters. The search was performed using 1000 random additional sequences. Subsequently, the most parsimonious trees (MPTs) were subjected to and additional round of TBR to further explore the tree-space.

After the first phylogenetic analysis confirmed the inclusion of ML 357 within Ankylopollexia, the specimen was added to the dataset of Xu *et al*., (2018)in order to explore its affinities within the clade. We corrected the scoring for character 121 of *Dryosaurus altus*, *Dysalotosaurus lettowvorbecki* (scored as: 0), *Valdosaurus canaliculatus* and *Uteodon aphanoecetes* (scored as: ?) based on a literature review (Galton, 1981, Carpenter & Wilson, 2008, Barrett et al., 2011, Barrett, 2016). As a tree-search strategy, it was performed a heuristic search with 1000 replicates, keeping 10 trees per replicate. The MPTs were then subjected to the TBR algorithm as in the previous search.

We investigated the variation of evolutionary rates across the topology obtained by the analysis of the dataset of Xu *et al*. (2018). We utilized the script for TNT developed by Rauhut & Pol (2019) to calculate the Homoplasy Concentration (HC) index, which is linearly related to increase in evolutionary rates. The ages (FAD/LAD) of terminal taxa were downloaded from the ~~by~~ Paleobiology Database on the 19/01/2021, inserting the term Iguanodontia, and in case of multiple contradictory entries, it was chosen the age range with the highest number of entries.

As an additional line of evidence, we performed a third set of analysis using Bayesian inference. We re-analysed the dataset of Xu *et al*. (2018) in the program Mr.Bayes v.3.2.7 (Ronquist *et al*., 2012) in two steps: first, we performed a non-clock analysis to calculate background evolutionary rate, and then we proceeded to a Clock Analysis, time-calibrating the topology recovered from the Non-Clock analysis. The character evolution followed Mk model (Lewis, 2001) and the values were sampled from a gamma distribution. The analysis sampled 10 000 000 of generations per run, sampled ~~under~~ with Markov-Chain-Monte-Carlo (MCMC) method for 4 runs of 6 chains per run. The initial "burn-in" was set at 25%. Convergence of independent runs and stationarity was assessed through the program Tracer v.1.7.1 (Rambaut *et al*., 2018) ~~,~~considering effective sample size (ESS) for each parameter informative with values equal or > 200. Then we proceeded to the clock-analysis according to the Fossilized Birth-Death Model (FBD) Heath *et al*., (2014), under maximum diversity sampling tree methods corrected to exclude sampled-ancestor model. The topology recovered from parsimony and non-clock analysis was implemented as strict prior. It ~~was~~ employed the relaxed uncorrelated clock model IGR and the background values for the clock-rates were sampled by a lognormal distribution. As in the previous analysis, character evolution followed the Mk model (Lewis, 2001) and the values were sampled from a gamma distribution. The analysis sampled 10 000 000 of generations per, sampled ~~under~~ with

Markov-Chain-Monte-Carlo (MCMC) method for 4 runs of 6 chains per run. The initial "burn-in" was set at 25%. Convergence and stationarity were again assessed in Tracer v.1.7.1, adopting the same criteria described in the non-clock analysis. We provided a soft root upper prior (220, 205) for the tree, lower than the stratigraphic occurrence of the outgroup taxon (*Lesothosaurus diagnosticus*) and being ~~coherent~~ consistent with the ghost lineage of Ornithischia inferred by ~~in~~ other works (Baron, 2019). Since Mr.Bayes needs an extant taxon to perform the calculation of evolutionary rates, we set the occurrence interval for *Lesothosaurus diagnosticus* as (10, 0 Ma). We opted for this operation instead of creating a dummy taxon coded for just 0 because the matrix of Xu *et al.,* (2018) is designed in a way that *L. diagnosticus* has ~~such~~this coding. Therefore, the adding of a dummy taxon would create noise in the topology and the rooting. ~~We followed~~ Following Simões *et al*. (2020a,b), we implemented informative prior for the base of the clock rate. This prior value is obtained subdividing the median value for tree length in substitutions from posterior trees by the age of the tree, based on the median of the distribution for the root prior (4.0714/205.5= 0.02), following Simões *et al*. (2020).

~~as the base of the clock rate was given an informative prior as previous non-clock analysis - the median value for tree length in substitutions from posterior trees divided by the age of the tree based on the median of the distribution for the root prior (4.0714/205.5= 0.02).~~

Moreover, we modelled rate~~d~~s according a lognormal distribution. The rates sampled from the lognormal distribution, the mean of the lognormal distribution was given the value based on the non-clock tree estimate (0.02) in natural log scale = - 3.9120. We chose to use the exponent of the mean to provide a broad standard deviation ($e^{0.02}$ =1.0202). The terminal age uncertainty of the previously downloaded FAD/LAD was modelled according to a uniform prior.

In the attempt to reconstruct body length of the specimen ML 357, we used the linear equations introduced by Becerra & Ramirez (2018). We opted for the ones derived for the metatarsal III, since it is the most complete and unaltered appendicular element in ML 357. In addition, Becerra ~~and~~ & ~~Martinez~~ Ramirez (2018) categorized ornithischian dinosaurs' locomotory models as (i) cursorial, (ii) sub-cursorial and (iii) gravi - portal, based on the ratio of the femur and whole leg length. Ornithopods (including hadrosaurs) are considered to range from cursorial to sub-cursorial locomotion stance. Since the hindlimb of ML 357 is not preserved in its integrity, we estimated the body length of ML 357 assuming first a fully cursorial locomotory model according to the equation (1):

$$bl = -147.18 + 17.45 \times (m3)$$

Secondly, sub-cursorial locomotory model according to equation (2):

$$bl = -441.11 + 24.54 \times (m3)$$

Where bl is the estimated body length and m3 is the linear measurement of the metatarsal III. The ecological implications of both models are discussed below, in the ~~discussion section~~Discussion. Selected measurements of ML 357 are provided in Tab.1. Supporting information includes: TNT files of the parsimony analyses (S2, S39), the infiles of the Non-Clock (S4) and Clock- Analysis (S5) and 3D model of the leg of ML 357 (S6)

	Height	Mesio distal width	Labiolingual width				
Complete maxillary tooth ML 357-31	16	10	6				
Maxillary crown tooth ML 357-31	11	9	9				

	Total Length	Centrum cranial mediolateral width	Centrum cranial dorsoventral heigth	Centrum caudal mediolateral width	Centrum caudal dorsoventral heigth	Neural spine height	Neural arch mediolateral width
Caudal vertebra n.1 ML 357 - 9	59	58	52	55	56	56	80
Caudal vertebra n.2 ML 357 - 10	47	48	53	47	52	45	60
Caudal vertebra n.3 ML 357 - 11	47	44	48	40	50	45	60
Articulated carpus	Total Length	Mediolateral width	Craniocaudal heigth				
Metacarpal (fragment) ML 357 - 5	32						
Carpal n.1 ML 357 - 5		20	22				
Carpal n.2 ML 357 - 5		13	13				
Carpal n.3 ML 357 - 5		14	18				
		Mediolateral distal width	Extensor-palmar distal heigth				
Distal metacarpal 1 ML 357 - 25	23	18	6				
Distal metacarpal 2 ML 357 - 26	18	18	16				
Left manual elements		Mediolateral distal width	Mediolateral proximal width	Dorsovental distal heigth	Dorsovental proximal heigth		
Manual phalanx n.2 ML 357 - 22	8	15	18	10	10		
Manual phalanx n.3 ML 357 - 21	17	16	19	10	13		
Manual phalanx n.4 ML 357 - 24	19	18	20	9	15		
Manual ungual n.1 ML 357-1	35		22		15		
Manual ungual n.4 ML 357 - 23	38		15		15		
Right manual elements							
Manual phalanx n.1 ML 357 - 4	17	17	22	10	17		
Manual ungual n.2 ML 357 - 2	30		17		15		
Manual ungual n.3 ML 357 - 3	33		12		14		
Manual ungual n.5 ML 357 - 20	33		18		13		
	Total Length	Mediolateral distal width	Medial condyle length	Lateral condyle length	Flexor groove width	Extensor groove width	
Femur ML 357 - 6	280	120	120	110	50	30	
	Total Length	Craniocaudal distal width	Mediolateral width				
Tibia proximal epiphysis ML 357 - 7	210	140	135				

	Total Length	Mediolateral distal width					
Tibia distal epiphysis ML 357 - 12	210	150					
	Craniocaudal length	Craniocaudla length					
Fibula (proximal) ML 357 - 8	75	90					
Pes ML 357 - 12							
	Mediolateral Width	Dorsoventral heigth					
Tarsal 3 ML 357 - 12	50						
Tarsal 4 ML 357 - 12	70						
Astragalus ML 357 - 12	90	50					
Calcaneum ML 357 - 12	30	70					
	Total Length	Mediolateral distal width	Mediolateral proximal width	Dorsoplantar distal heigth	Dorsplantar proximal heigth		
Metatarsal I ML 357 - 12	30*						
Metatarsal II ML 357 - 12	140	50	25	45			
Metatarsal III ML 357 - 12	175	70	40	40			
Metatarsal IV ML 357 - 12, 18	60*	35	70	45			
Pedal Phalanx II-1 ML 357 - 17	50*		48		55		
Pedal Phalanx II-2 ML 357-14	40	30	45	20	40		
Pedal Phalanx III-1 ML 357-13	63	45	69	25	45		
Pedal Phalanx III-3 ML 357 - 15	35	35	28	20			
Pedal Ungual II ML 357 - 16	60	25		30			
Pedal Ungual III ML 357 - 19	60	30		25			

Tab.1: selected measurements of ML 357. All measurements are in mm.

Results

Systematic palaeontology

Dinosauria Owen, 1842

Ornithischia Seeley, 1887

Ornithopoda Marsh, 1881

Iguanodontia Sereno, 1986

Dryomorpha Milner & Norman, 1984

Ankylopollexia Sereno, 1986

Styracosterna Sereno, 1986

Draconyx loureiroi Mateus & Antunes, 2001

Figures 2-7

Type material: the holotype specimen (new reported material marked with *), ML 357 (subnumbers from 1 to 31)includes two maxillary teeth, carpal bones, two metacarpal distal ends*, three left carpal phalanges, one right carpal phalanx*, two left unguals, three right unguals*, and right leg including proximal femoral epiphysis, proximal and distal epiphysis of the tibia, astragalus, calcaneum, four metatarsals, five phalanges and two unguals.

~~*Previously referred*~~*Referred specimen*: an isolated left femur, ML 434 ~~proceeding~~ from 1 km south of the type locality previously referred to *Draconyx loureiroi* by Mateus & Antunes (2001), now referred to Ankylopollexia indet.

Type locality, horizon and age: Vale de Frades, Lourinhã Municipality, Portugal. Praia Azul Member of Lourinhã Formation, lower Tithonian, 151-152 Ma.

Emended diagnosis: styracosternan iguanodontian distinguished from other basal iguanodontians by the following combination of characters: unfused and ~~unpacked~~ non interlocked carpus; absence of a sharp crest running from the medial condyle of the femur towards of the lesser trochanter, fully open u-shaped extensor groove on distal epiphysis of femur; fully open V-shaped flexor groove without overhangs on distal epiphysis of the femur;

concave medial margin of proximal epiphysis of tibia; caudally pointing fibular condyle of tibia; a splinter-like metatarsal I.

Description and comparisons

Cranial material

~~Hereinafter we opt to make to follow the description of each bone by a separated remark and comparison section, for the sake of readability of the text.~~

Maxillary teeth (ML 357-31) (Fig.2 A-B)

One of the maxillary teeth preserves part of the root (Height:16 mm, Labiolingual Width: 6), and ~~the~~ its crown is complete (Fig.2-A) the other one is just an isolated crown (Fig.2-B). The specimens appear to have suffered some erosion and post-mortem breakage. The root is slightly labio-lingually curved and tapers smoothly into the crown (Fig. 2-A). There is no cingulum at the junction between the root and the crown~~The contact between the crown and the root does not present a cingulum~~. Overall, the crown is leaf-shaped, the veneer of enamel is thicker on the labial side (Fig. 2-A). Labially a thick primary ridge is distally off-set and five accessory ridges are present on the mesial surface(Fig. 2-A,B). Non-mammilated hook-like denticles are coarsely present on the mesial crown margin, while distally they appear to have been obliterated by either erosion or ~~the mastication process~~occlusal wear. An extensive occlusal surface develops ~~in apical-most part~~on the apex of the crown and is inclined labio-lingually approximately around 30 degrees (Fig. 2-A,B).

Remarks - the tapering root, slightly labiolingually recurved and the leaf-shaped crown is a common characteristic of Dryomorpha (Galton, 1983, 2006; Norman, 1986, 2004). The maxillary crowns possess a distally offset primary ridge resembling the condition of ~~Ankylopollexia~~ ankylopollexians but ~~,~~ differing from ~~Dryosauridae~~ dryosaurids in which the

primary ridge is located towards the center of the crown (Galton, 2006). In the original description, Mateus ~~and~~ & Antunes (2001) indicated the presence of five accessory ridges in the distal half of the crown as an autapomorphy ~~for~~ of *Draconyx loureiroi.* However, the number of accessory ridges ~~change~~ is variable throughout the dental series (Galton, 2006); therefore, we here regard it as a non-informative character if the tooth is not found articulated in its tooth position.

Axial Skeleton

Caudal vertebrae (ML 357 9-11) (Fig.3 K-M, Fig. ~~43~~ A-F)

Three proximal caudal vertebrae are preserved and, as for the rest of the skeleton, they have suffered breakage and erosion. ~~They are located in proximal region of the caudal series.~~ The centra are stout and ~~,~~ craniocaudally compressed. The largest centrum is ML 357 – 9 , while ML 357 – 10 and ML 357 -11 are slightly smaller. The cranial and caudal surfaces are slightly amphicoelous, having a sub-elliptical rounded shape (Fig.~~43~~ A, C, G, I, M, O). Dorsally, the neural arch preserves the ventral-most portion of the neural spine. Immediately caudal to the spine, in the most complete specimen ML 357-9,10,(Fig.~~43~~ C, O) two small, rounded and steeply inclined post-zygapophyses ~~depart~~ diverge laterally. On the lateral surface of the neural arch, the articulation for the transverse processes is overlai~~d~~n by a ~~breakage~~ broken surface. The presence of ~~such~~this surface indicates that these ~~preserved~~ vertebrae represent the cranial-most portion of the caudal series. In ~~the~~ ventral view, the centra have an hourglass shaped outline (Fig.~~43~~-E, K, Q). The ventral surfaces of the centra possess a narrow keel and the margin is highly concave (Fig. ~~3~~4-B, P) . Caudally, broad ~~insertions~~ facets for chevrons are present.

Remarks - The three caudal vertebrae are stout and cylindrical, similar in overall shape and proportions to those of other basal iguanodontians such as: *Dryosaurus altus, Dysalotosaurus lettowvorbecki, Camptosaurus dispar, Cumnoria prestwichii, Uteodon aphanoecetes* and

Mantellisaurus atherfieldensis (Galton and Powell, 1980; Galton, 1981; Norman, 1986; Carpenter and Wilson, 2008; Carpenter and Galton, 2018). On the other hand, they do differ remarkably ~~by the ones~~from those of *Iguanodon bernissartensis* and *Iguanacolossus fortis* in being less discoidal in shape, and from *Barilium dawsoni* by being less compressed dorsoventrally (Norman, 1980, 2011; McDonald et al., 2010b).

Manus (ML 357 – 1-5, 20-26) (Fig. 45)

The partial carpus (ML 357-5) is composed by the proximal ~~most~~ part of a metacarpal, two distal carpals and a proximal carpal (Fig. ~~4~~5 A). Two isolated distal ~~most~~ epiphyses of metacarpals (ML 357 – 25, 26) are associated with the semi-articulated carpus, being ~~coherent~~ consistent in size and state of preservation (Fig.5 ~~4~~ F,G). Four manual phalanges and five ungual phanlanges are associated with~~to~~ the carpus (Fig. ~~4~~5 B-E). Three manual phalanges (phalanx n.2 ML 357 - 22 , phalanx n.3 ML 357 - 21 and phalanx n.4 ML 357 - 24) and two unguals (ungual n.1 ML 357-1 and ungual n.4 ML 357 - 23) are ~~interpreted~~ likely to belong to left manus (Fig. 4 , while the remaining three unguals (ungual n.2 ML 357 - 2 , ungual n.3 ML 357 - 3 and ungual n.5 ML 357 - 20) and manual phalanx n.1 ML 357 - 4 are ~~interpreted to belong~~ attributed to the right manus. Given the fragmentary condition and the weathering of the specimen, it is not possible to identify each individual carpal bones. The two distal carpals are cuboid in shape and are very stout elements, while the proximal carpal is more lightly built and slightly arched (Fig. 54A). The proximal end of the metacarpal preserves a concave proximal margin~~. Beside the non-favourable condition of~~ Despite of the poor preservation of the specimen, it is possible to ~~assess~~ determine that ~~the fact~~ the carpus does not ~~present~~include ~~-~~fused elements, ~~being~~ as all of the contacts between all the identifiable carpals are ~~widely marked~~ visible (Fig. 54A).

The two isolated distal metacarpals fragments are similar in shape; they are compressed along their extensor-palmar axis, broadening medio-laterally towards their distal ends. The medial and lateral ~~condyles~~ ginglymi are sub-equal in size and preserves on their ~~medial and lateral margin the scar insertion for tendons~~collateral ligament pits.

The m~~M~~anual phalanges ~~here numbered as phalanx~~ ML 357 - 22 and ~~phalanx~~ ML 357 - 21, articulate~~s to one another~~with each other. Further~~more~~, phalanx ML 357 - 22 articulates with the ungual ~~n.4~~ ML 357 - 23~~,~~; therefore, these latter manual elements compose a complete ~~manual~~ finger (Fig.4~~5~~ C,D,K). In general, all of the phalanges have a distal triangular section, moderately arched ventral surface, and strongly inclined and robust ~~medial condyles~~ginglymi. The lateral ~~condyle~~ ginglymus is ~~in these specimens is sensibly~~ smaller ~~in size~~ respect to the medial one, with the exception of the phalanx n.2 where they are sub-equal (Fig. 54B-E). The unguals are generally elongated and claw-like, being slightly arched along extensor-palmar axis and having and sub-triangular articular facet (Fig. 54 H-L). The only exception ~~is constituted by~~ the ungual n.5 (Fig. 54L) that, instead, appears to be compressed along its extensor-palmar axis. A fracture develops medio-laterally~~,~~ is slightly inclined cranio-caudally, and the two parts separated by this fracture have suffered medio-lateral displacement.

Remarks - despite ~~the~~ poor preservation of ~~this element,~~ the carpus of ML 357 shows features that allow comparisons with other taxa. The small ~~preserved~~ metacarpals are not significantly different from those of other iguanodontians (Norman, 2004). The carpus, however, is constituted by isolated blocky elements, resembling the condition in ~~of~~ dryosaurids and *Tenontosaurus* spp. (Dodson, 1980; Galton, 1981; Forster,1990; Winkler et al., 1997). ~~instead~~The distal carpals of ML 357 differ from the ones of *Camptosaurus dispar*, which are arranged ~~of the~~ in two co-ossified ~~blocks co-ossified~~ and ~~condition~~highly interlocked blocks

(REVISE). Furthermore, the carpus ML 357 does not exhibit ~~seen in *Camptosaurus dispar* or~~ the total ~~ossification~~ossified condition present in *Iguanodon bernissartensis*, *Magnamanus soriaensis, Mantellisaurus atherfieldensis* and other styracosternans~~-~~) (Fig.12 A-J) (Dodson, 1980; Norman, 1980, 1986, 2004, 2011, 2015, Fuentes Vidarte). The carpals and the manual unguals ~~differ~~ are similar ~~from~~ to the ones present in *Camptosaurus dispar*, *Uteodon aphanoecetes*, *Cumnoria prestwichii*, differing from the ones of ~~and other~~ more derived styracosternans (i.e. *Mantelissaurus atherfieldensis*, *Iguanodon bernissartensis*, *Magnamanus soriaensis* and all other hadrosauriformes) in being respectively more arched and ~~or~~ more claw-like instead of extremely compressed and hoof-like (Fig.12 A-J) (Norman, 1980,1986, 2004; Galton & Powell, 1980; Carpenter & Wilson, 2008, Vidarte et al., 2010).

Femur ML 357 - 6 (Fig.3 A-E, ~~5~~6 A-E)

The preserved right femur consists of the heavily eroded distal-most part of the shaft and the distal epiphysis~~, which are heavily eroded~~. The proximal-most part of the preserved shaft is mediolaterally crushed and compressed, due to taphonomic processes~~ompressed~~. The femur is strongly bowed ~~antero-posteriorly~~cranio-caudally, the section of the shaft was sub-circular, but it is heavily distorted proximally by the compression, and damaged distally (Fig.~~5~~6 B,D). The distal epiphysis is sub-rectangular in shape in distal view, extending slightly more medio-laterally than cranio-caudally. The two distal condyles are preserved, appearing sub-equal in size with the lateral condyle slightly larger than the medial one (Fig.6~~5~~ E). A deep, extensive, fully-open, and U-shaped ~~A deep and extensive, fully open~~ extensor groove separates the two condyles cranially~~, having its margins arranged into a V-shape~~ (Fig.~~5~~6 E)~~.~~. The ~~anterior~~ cranial process of the ~~lateral~~ lateral condyle is rounded, ~~deflecting~~ deflected ~~posteriorly~~caudally. ~~, and forming the lateral scar for tendon insertion.~~ The ~~posterior~~ caudal finger-like process of the lateral condyle (condylid, according to Bertozzo *et al.*, 2017) is not

preserved, being broken at its base, but the crest for the muscular insertion is distinguishable. The medial condyle appears stout and rectangular, although its cranial ~~anterior~~ and caudal ~~posterior~~ process have been eroded. The flexor groove is fully open and its margin, consisting of the caudal process of the lateral condyle and the condylid of the medial condyle, are V-shaped in outline.

Remarks - The preserved femoral shaft ~~preserved~~ is strongly bowed cranio-caudally, as in dryosaurids, most ~~of~~ elasmarians, *Camptosaurus dispar*, ~~*Cumnoria prestwichii*~~, and differently from *Tenontosaurus* sp. and other styracosternans (Norman, 1980, 1986, 2004; ~~Galton & Powell, 1980;~~ Carpenter & Galton, 2018; Carpenter & Wilson, 2008; Herne *et al.*, 2019; Rozadilla *et al*., 2019, 2020). On the cranial surface there is not any crest developing from the medial condyle, extending proximally towards the lesser trochanter, as it occurs in other ankylopollexians, such as *Camptosaurus dispar*, *Uteodon aphanoecetes*, *Mantellisaurus atherfieldensis* and *Iguanodon* sp. (Gilmore, 1909; Norman, 1980, 1986, 2004; Carpenter & Wilson, 2008; Carpenter & Galton, 2018). – The lateral condyle of the distal epiphysis of the femur in *Draconyx loureiroi* is concave in outline, and it extends more cranio-caudally than the ones of *Uteodon aphanoecetes*, *Cumnoria prestwichii* and *Camptosaurus dispar* (Fig.7) (Galton & Powell, 1980; Carpenter & Wilson, 2008; . Moreover, the inflection point of the curvature is located more cranially in *Draconyx loureiroi* than in *Camptosaurus dispar* and *Uteodon aphanoecetes* (Carpenter & Wilson, 2008; Carpenter & Galton, 2018), while *Cumnoria prestwichii* exhibits a smoother outline without abrupt changes in curvature. The lateral condyle of Early Cretaceous species such as *Barilium dawsoni* and *Mantellisaurus atherfieldensis* are larger in proportions with the respect to the total size of the epiphysis, and extend more caudal than the ones of the above-mentioned taxa, including *D.loureiroi* (Norman, 1986; 2011). The medial condyle of

Draconyx loureiroi is sub-rectangular, and its medial margin is straight as in the one of *Mantellisaurus atherfieldensis* and *Barilium dawsoni* (Norman, 1986; 2011). On the contrary, in Jurassic taxa such as *Uteodon aphanoecetes* and *Camptosaurus dispar* the medial margin of the medial condyle is rounded (Carpenter & Wilson, 2008; Carpenter & Galton, 2018).

The flexor and extensor grooves are fully open as in many basal and cursorial iguanodontians, ~~differently~~ contrasting with ~~from~~ more derived forms (Norman, 2004). Extensor grooves of the Jurassic taxa *Camptosaurus dispar* and *Uteodon aphanoecetes* and are fully open, but shallower compared to the ones of *Draconyx loureiroi*, *Cumnoria prestwichii, Mantellisaurus atherfieldensis*, *Barilium dawsoni* and *Iguandon* sp. (Norman, 1980, 1986, 2004, 2011, Carpenter & Wilson, 2008; Carpenter & Galton, 2018, Verdù *et al.*, 2018). Moreover, the flexor grooves walls of *Cumnoria prestwichii* and *Uteodon aphanoecetes* are slightly divergent from one another (Fig. 7). The extensor groove of the Early Cretaceous iguanodontians *Barilium dawsoni* and *Mantellisaurus atherfieldensis*, and other styracosternans are partially enclosed by over-hangs of medial and lateral condyles. ~~Contrarily to most large-sized ankylopollexians,~~ *Draconyx loureiroi* does not exhibit~~there is no~~ an overhang of the medial condyle on the flexor groove, unlike the condition present in *Uteodon aphanoecetes*, *Camptosaurus dispar*, *Cumnoria prestwichii*, *Mantellisaurus atherfieldensis* and *Ouranosaurus nigeriensis* (Norman, 1980, 1986, 2004, 2011, Carpenter & Wilson, 2008; Bertozzo *et al.*, 2017; Carpenter & Galton, 2018, Verdù *et al.*, 2018). This condition more closely resembl~~es~~~~ing~~ the plesiomorphic condition within Ornithopoda (Norman *et al.*, 2004).

Tibia (ML 357 – 7,12) (Fig. 3 F-G, Fig. 6 ~~5~~ F-J, Fig.~~6~~8 A-D)

The proximal (Fig.~~6~~5 F-J) and distal (Fig.~~6~~8 A-E) epiphyses of the tibia are preserved, but the tibial shaft is missing. Both extremities ~~appear~~ are heavily eroded and covered ~~in~~ by matrix

and adhesives, but relevant characters are still distinguishable. The proximal epiphysis preserves a conspicuous cnemial crest, a robust fibular condyle and the internal condyle. The cnemial crest tapers dorsally forming a smooth edge~~;~~, in dorsal view its margins are laterally concave and medially convex (Fig.~~5~~6 G,I). Laterally, it is divided by the fibular condyle ~~concave by~~to form a deep and extensive scar (sulcus tibialis). The fibular condyle is a stout process that deflects strongly caudally, its articular facet is rounded, and it blends smoothly with the anterior and posterior surfaces of the condyle. The internal condyle is a blunt eminence directed caudally and~~,~~ ~~deflecting~~ projecting gently laterally. As with the cnemial crest, its lateral margin is concave while the medial margin~~ly~~ is strongly convex (Fig.~~5~~6 E). This convexity forms a deep sulcus, which separates the internal condyle from the fibular condyle. Immediately ventral to the proximal epiphysis the proximal ~~most~~ part of the diaphyseal shaft is preserved, and it is ~~teardrop in shape~~teardrop shaped in cross~~-~~-section. The distal part of the tibia is articulated with the astragalus, calcaneum and the metatarsals (Fig.~~6~~8 A-E). The distal epiphysis flares mediolaterally, the medial malleolus is rounded and slightly more expanded medio-laterally, than the lateral one, which is ~~pointier~~narrow and elongate, expanding~~.~~ proximo-distally. They articulate between each other forming an angle of approximately 45°. The intermuscular line is located on the caudal surface of the distal epiphysis, separating the surface of the two malleoli. It reaches the astragalus, forming with its apex a continuous concave surface.

Remarks - the medial margin of the proximal epiphysis of the tibia is convex as is typical~~ly~~ ~~found in~~of many iguandontians (Norman, 2004), except for *Talenkauen santacrucensis* and *Eousdryosaurus nanohallucis* (Escaso *et al*., 2014; Rozadilla *et al*., 2019; Dieudonné *et al*., 2020). As noted by Dieudonné *et al*. (2020), the cnemial crest apex~~edge~~ is directed strongly cranio-laterally, a characteristic common to Laurasian d~~D~~ryomorphans and *Dysalotosaurus*,

differing from the condition exhibited by Elasmaria and the Portuguese ornithopod *Eousdryosaurus nanohallucis* (Escaso *et al*., 2014). As in many ~~styracosternans~~styracosternans, the cnemial crest is well developed (Norman, 2004). The fibular condyle differs from dryosaurids (with the exception ~~for~~ of *Valdosaurus canaliculatus*), *Camptosaurus dispar, Uteodon aphanoecetes* in being partially posterolaterally deflected, similarly to the condition seen in *Cumnoria prestwichii*, *Talenkauen santacrucensis* and more derived styracosternanans (Galton & Powell, 1980; Norman, 1980 1986, 2011; Norman *et al*., 2004; Carpenter & Wilson, 2008; Barrett *et al*., 2011; Rozadilla *et al*., 2019) . The distal epiphysis, found in articulation with the rest of the pes, does not differ significantly from that of other iguanodontians (Norman, 2004).

Fibula (ML 357 – 8,12) (Fig.3 I, J, Fig.6~~5~~ F-J, Fig.~~6~~8 A-D)

The distal and proximal epiphyses of the fibula are preserved, ~~while~~ whereas the diaphysis is completely ~~lacking~~absent. The proximal end is a flattened sub-triangular element.~~,~~ ~~–~~Dd~~d~~orsally it appears to be slightly medially convex. The cranial margin deflects abruptly dorsally into the cranial process, which is slightly eroded (Fig. 6 ~~5~~I). The caudal margin, on the other hand, deflects less abruptly dorsally. On the lateral surface, close to the caudal margin, a deep fossa is present.

The distal epiphysis is in articulation with the rest of the pes, located on the lateral surface of the tibia, and contact~~ings~~ the calcaneum (Fig.~~6~~7 A-D).

Remarks - the proximal epiphysis ~~of fibula presents~~exhibits cranial and caudal margins that diverg~~inge~~ smoothly as ~~like~~ in *Dryosaurus altus*, *Dysalotosaurus lettowvorbecki, Eousdryosaurus nanohallucis, Valdosaurus canaliculatus* and *Talenkauen santacrucensis* , but differing~~differently~~ from *Iguanodon bernissartensis*, *Ouranosaurus nigeriensis* and

Mantellisaurus atherfieldensis (Norman, 1980,1986; Galton, 1981; Barrett *et al*., 2011; Barrett, 2016; Bertozzo *et al*., 2017; Escaso *et al*., 2014; Rozadilla *et al*., 2019). As in *Talenkauen santacrucensis* and *Sektensaurus sanjuanboscoi* the caudal margin of the proximal part of the fibula is almost vertical (Ibiricu *et al*., 2019; Rozadilla *et al*., 2019).

Pes (ML 357 – 12-19) (Fig.3 N, Q, Fig.~~6~~8 A-F, Fig. 9~~7~~ C-D)

The pes was found in articulation~~,~~ with the distal tibia, distal fibula, astragalus and calcaneum, and proximal metatarsals ~~strongly bounded together~~. The ~~heavy~~ diagenetic permineralization between the tibia and the rest of the pes prevented a reliable segmentation by CT techniques ~~preventing CT techniques to allow a reliable bone segmentation~~. ~~Such conditio~~This also ~~n~~ hampered the views of the internal anatomy~~ical perspective~~ of the astragalus and calcaneum. The articulated elements share ~~all~~ the same sub-number (ML 357 – 12), while the isolated elements have their own numbers. Therefore, the same element may have two sub-numbers depending if ~~the~~ a part of it belongs to the articulated block or not.

Calcaneum

The calcaneum is preserved in its entirety, and ~~it~~ does not show signs of significant breakage, erosion or distortion ~~(Width: 30, Heigth: 70)~~. In its general appearance, the calcaneum is a compact and narrow element, expanding cranio-caudally more than medio-laterally (Fig.8~~6~~ B, E). Distally, its surface is sub-rectangular outline and it extends dorsally, appearing as a small rhomboidal element in caudal view (Fig.8~~6~~ B, E). Caudally, the medial margin of the calcaneu~~s~~m forms a smooth concavity that accommodates the~~a~~ lateral-most margin of the astragalus. In lateral view, the calcaneum appears ~~to be~~ triangular ~~having the highest vertex located caudally~~with a caudal apex, and slightly deflected~~ting~~ proximally. The proximal and distal margins progressively flare cranially, with the latter forming a ~~scoup~~scoop-like concavity.

Astragalus

The astragalus, as with the calcaneum, is complete and not significantly distorted or eroded. In distal view, the bone has a sub-trapezoidal shape (Fig.~~6~~8 A, E). Laterally, it contacts the medial malleolus of the tibia ~~with~~ via a deep concavity, while medially the astragalus/calcaneum contact is ~~a~~ straight ~~line~~ (Fig.~~8~~6 A, E). In caudal view, the astragalus is triangular, with a high ascending process representing the apex~~appears as a triangular element, being the apical vertex constituted by a high ascending process~~, which protrudes extensively dorsally. Immediately ventral to the ascending process, ~~A~~a stout steeply inclined caudo-medial process, ~~inclined caudo-medially,~~ forms a well distinguishable relief.

Remarks - the astragalus of ML 357 is sub-triangular and its caudal surface is moderately high as in dryosaurids, *Camptosaurus dispar, Cumnoria prestwichii, Uteodon aphanaecetes, Mantellisaurus atherfieldensis*~~,~~ and *Iguanodon bernissartensis* ~~and~~ (Norman, 1980, 1986; Galton & Powell, 1980; Galton, 1981; Carpenter & Wilson, 2008; Barrett et al., 2011). The ascending process is not as developed as in *Iguanodon bernissartensis*, *Mantellisaurus athefieldensis* or *Barilium dawsoni* (Norman, 1980, 1986, 2011), more closely resembling the condition in ~~resembling more the condition of~~ *Cumnoria prestwichii*, *Uteodon aphanoecetes*, *Camptosaurus dispar* (NMNH~~M~~ 2210) and *Ouranosaurus nigeriensis* (Galton and Powell, 1980; Carpenter and Wilson, 2008; Bertozzo et al., 2017). As in the other Portuguese ornithopod, *Eousdryosaurus nanohallucis,* it shows a caudomedial process, which casts ~~casting a~~ doubt on the diagnostic status of this character for this latter taxon (Escaso *et al*., 2014). The calcaneum does not ~~present~~possess any remarkable differences from other ankylopollexians (Norman, 2004).

Distal tarsals~~Tarsus~~

Two distal tarsals are preserved, which are identified as tarsal 3 and tarsal 4 (Fig. ~~6~~8 D). Tarsal 3 is a large element ~~being~~ that is mediolaterally elongated and contacts ~~ing~~ metatarsal 3 ~~with~~ along a straight and linear surface (Fig. 8~~6~~ D). Tarsal 4 is a stout, elongated element ~~(Width: 70)~~, and contacts the metatarsal IV ~~through~~ along a concave surface, while its medial-most tip overlaps ~~proximally the~~ tarsal 3 proximally (Fig. ~~6~~8 D).

Remarks -~~The~~ distal tarsals 3 and 4, found in articulation with metatarsal III and IV resemble the 'cushion-like' condition described by Gilmore (1909) ~~for~~ in *Camptosaurus dispar*, differing from the thin-like and sub-rounded condition ~~found~~ in *Mantellisaurus atherfieldensis* and *Iguanodon bernissartensis* (Norman, 1980, 1986) or the one present in in basal ornithopods (Galton, 1974, 1981)~~the 'lower ornithopods', as described by Galton (1974, 1981).~~

Metatarsus

~~The metatarsus appears to be elongated and slender, preserving I-IV metatarsals~~Although they are fragmented, metatarsals II-IV are long and slender (Fig. ~~6~~8, ~~7~~9 C-D). ~~The metatarsus appears to have suffered a severe fragmentation process, although the general structure is preserved. Metatarsal II-IV are preserved, and a~~ A thick splinter of bone next ~~of~~ to metatarsal II ~~has been~~was interpreted as the proximal--most part of the metatarsal I in the original description of Mateus ~~and~~ & Antunes (2001), and a 'vestigial digit I' has been proposed as possible autapomorphy for ~~the species~~ *Draconyx loureiroi*. Despite being heavily eroded, the bone is preserved in anatomical position, and the rod-like structure supports the interpretation of ~~such~~ this bone as the first metatarsal (Fig. 8~~6~~ F). The status of this character as an~~such a character as~~ 'autapomorphy' is discussed below. A deep groove ~~in continuity~~ in continuity

with this fragment and impressed on metatarsal II likely represents the entire articulation surface with metatarsal I~~with the fragment is impressed on the metatarsal II, representing probably the entire length of the complete bone~~ (Fig. ~~6~~8 F).~~. Metatarsals II-IV are undoubtedly identifiable as such and are in better state of preservation.~~ Metatarsals II and III are complete and they do not appear to have suffered extensive breakage and fracture (Fig. 8~~6~~ C-D). Metatarsal IV ~~instead,~~ is broken at midshaft and the distal epiphysis is preserved as an isolated element.

Pedal digit I

The first pedal digit~~-~~ consists only of ~~is constituted by~~ the ~~sole~~ splint like metatarsal I ~~(Total Length: 30 mm)~~ (Fig. 8~~6~~ F).

Pedal digit II

P~~The p~~edal digit II is represented~~preserved~~ by metatarsal II ~~(Total Length: 140)~~ , the pedal phalanx II-1 ~~(Total Length: 50)~~ (ML 357 – 17) and the ungual, phalanx II-2 ~~(Total Length: 60)~~ (357 – 16) which articulates with the phalanx II-2 ~~(Total Length: 40)~~ (357- 14). ~~The pedal~~Pedal phalanx II-1 is broken at mid-shaft, but the proximal and distal-most epiphyses are preserved (Fig.~~6~~ 8 A, C,D).

~~The me~~Metatarsal (Mt) II is positioned more proximally with respect to Mt III-IV. In medio-lateral view, metatarsal II has a keyhole shape, as described by Herne et al., (2018) for the Australian ornithopod *Diluvicursor pickeringi*, ~~being~~ with the proximal-most part dorsoplantarly higher than the distal epiphysis (Fig. ~~6~~8 A,F). The distal epiphysis develops more dorso-plantarly than medio-laterally, and the articular surface is convex. The shaft of M~~m~~t-II is piriform (teardrop) in ~~outline~~ cross-section, ~~being~~ with the plantar surface bearing a keel. The distal-most part of the epiphysis ~~develops~~ expands dorso-plantarly, ~~being~~ giving the

condyle a sub-trapezoidal ~~element~~ outline (Fig. ~~8~~6 A, D).~~.~~ The condyle of the metatarsal articulates perfectly with ~~the~~ pedal phalanx II-1, which accommodates the condyle in~~to~~ a gently convex triangular facet. The distal epiphysis of the phalanx is in articulation with ~~the~~ pedal phalanx II-2, which is a thick, sub-rectangular element in dorsal view (Fig. ~~6~~8 C-D). Proximally, the articular facet is not visible but distally the two condyles are well distinguishable being the lateral slightly inclined with respect to the medial one. On both lateral surfaces, deep extensor grooves are present for tendon insertion. The ungual (phalanx II-2) of the pedal digit II is preserved, being a ~~pointy~~ pointed claw-like element~~,~~ which is dorsoplantarly arched and proximodistally elongated (Fig. ~~6~~8 A, C-D).

Pedal digit III

P~~The p~~edal digit III is ~~constituted by~~composed of Metatarsal III ~~(Total Length: 175)~~, the largest pedal phalanx preserved ~~pd~~ III-1 ~~(Total Length: 63)~~ (ML 357 - 13), the smallest pedal phalanx, interpreted to be the ~~pd~~ III-3 ~~(Total Length: 35)~~ (ML 357 – 15) and the largest ungual, pedal phalanx III-4 ~~(Total Length: 60)~~ (ML 357-19). The pedal phalanx III-2 is missing. Metatarsal III is the longest element of the metatarsus, being a slender yet compact element. Proximally, the Mt-III articulates with the tarsal 3 and ~~incuneates~~ intervenes between M~~m~~t-II and M~~m~~t-IV (Fig. ~~8~~6 B-D). The sub-rectangular shaft end~~eulminate~~s distally ~~towards~~ in a mediolaterally-expanded condyle, ~~being~~ the only ~~one in the metatarsus~~metatarsal ~~presenting~~ exhibiting this condition. ~~The pedal~~Pedal phalanx III-1 is a stout, ~~and~~ robust element, which is moderately dorso-plantarly arched. The proximal articular facet is concave and sub-ellipsoidal in outline, being the ~~longest of the two axes, the one developing medio-laterally~~long axis oriented mediolaterally (Fig. ~~8~~6 B-D). Distally, the two ~~condyles~~ ginglymi are sub equal in size, being marked by deep ~~extensor grooves~~collateral ligament pits. ~~The p~~Pedal phalanx III-3 is a small proximo-distally compressed element, which possesses

presents a deep dorso-plantarly deep articular facet (Fig. 86 B-D). The ventral margin of pedal phalanx III-3 is not as arched as the other phalanges, and the extensor groovescollateral ligament pits occupy almost the totality of the entire lateral and medial surfaces. The ungual of the digit III (pedal phalanx III-3) is a stout and , pointyed element, being which is more robust than the ungual preserved on the pedal digit II. The ungual of digit III differs also from the other preserved ungual in having a less arched and more dorsoplantarly flattened outline (Fig. 86 B-D)..

Pedal digit IV

MThe metatarsal IV (ML 357 – 12, 18) (Total Length: 60) is the only element preserved of the pedal digit IV available. Proximally it is the most expanded mediolaterally expanded and dorsoplantarly compressed of the metatarsals, being and the proximal epiphysis is fan-shaped in dorsal/plantar view (Fig. 86 B-D). Distally, the section of the shaft becomes progressively sub-rectangular, culminating in into a moderately dorsoplantarly deep distal condyle (Fig. 86 B-D)..

Remarks - the metatarsus of ML 357 strongly differs strongly from those of *Camptosaurus dispar*, *Uteodon aphanoecetes*, *Iguanodon bernissartensis, Ouranosaurus nigeriensis* and other large-sized hadrosauriformes in general proportions, showing and has the slender and gracile proportions of seen in *Mantellisaurus atherfieldensis* and *Cumnoria prestwichii* instead (Gilmore, 1909; Norman, 1980, 1986, 2004, Galton & Powell, 1980; Bertozzo *et al.*, 2017). Furthermore, as in the latter taxa, ML 357 possesses a mMetatarsal III, which that is sensibly more elongated with respect to mMetatarsal II and IV (Galton & Powell, 1980; Norman, 1986). Differently fromIn contrast to elasmarians, *Dryosaurus altus*, *Dysalotosaurus lettowvorbecki, Cumnoria prestwichii* and *Camptosaurus dispar* the

mMetatarsal I is extremely reduced, losing any functional capability (Gilmore, 1909; Galton & Powell, 1980; Galton, 1981; Carpenter & Galton, 2018). On the other hand, this condition is preserved at least in some specimens of *Mantellisaurus atherfieldensis* and *Iguanodon bernissartensis* (Norman 1980, 1986). Assessing the presence of this character in other taxa is problematic, because of the extreme fragility of the reduced mMetatarsal I, whose absence/presence therefore is highly subjected to preservation bias. The allegedly dryosaurid *Eousdryosaurus nanohallucis* from the same fFormation as ML 357 has been shown to possess a reduced mMetatarsal-I -in articulation with a pedal phalanx (Escaso *et al*., 2014).

Previously referred specimens

Ankylopollexia indet.

Femur ML 434 (Fig.108)

Mateus & Antunes (2001) referred an isolated femur (ML 434) to *Draconyx loureiroi,* based on geographical proximity. The isolated left femur ML 434 is an almost complete and undistorted left femur but, lacksing part of the its proximal epiphysis and completely theall of its distal one. The femoral shaft is stout and robust in general proportions, and it appears strongly bowed cranio-caudally in lateral view, while but is straight in cranial view. The cross-section of the shaft is sub-ovoidal, presenting with a sharp edge in that correspondence corresponds with a the ridge that decurs extends dorsoventrally from the medial condyle. Proximally, the only a element preserved is part of the femoral head is preserved, which is that gently deflected medially. At approximately the mid-shaft on the medial surface of the femur, a pendant fourth trochanter is present, having its broad proximal base forming an elongated crest-like surface. The scar for the insertion of the Musculus M. caudifemoralis longus is located immediately cranial to the trochanter, being separated from the eminence of

the trochanter. Distally, the eroded epiphysis preserves the general appearance of the two condyles, although the ~~general~~ proportions with respect to one another are unclear. Parts of the flexor and extensor grooves are preserved caudally and cranially. A ~~W~~well-defined, sharp crest runs proximo-distally from the medial condyle towards to the location of the lesser trochanter.

Remarks - ~~The femur~~ ML 434 possesses a strongly cranio-caudally bowed femur and a pendant like fourth trochanter as in dryosaurids, *Camptosaurus dispar*, *Uteodon aphanoecetes* ~~and *Cumnoria prestwichii* a strongly cranio-caudally bowed femur and a pendant like fourth trochanter (Galton & Powell, 1980;~~ Galton, 1981; Carpenter & Galton 2018). The base of fourth trochanter is located ~~towardat~~s the midshaft of the femur, as commonly found in Ankylopollexia and different~~ly~~ from Dryosauridae, in which this structure is confined in the proximal part of the shaft (Norman, 2004). Similarly, to *Valdosaurus canaliculatus*, *Camptosaurus dispar*, *Uteodon aphanoecetes* and *Cumnoria prestwichii*, the scar of the Musculus caudifemoralis longus reaches the base of the fourth trochanter. Moreover, the morphology of the ridge formed by the base of the 4th trochanter is similar to the one of the specimen SHN.JJS.015 (Fig. 10~~8~~ A, D), which is not referable to *D. loureiroi* (Escaso, 2014) based on its~~the~~ partially enclosed flexor and extensor groove. The crest running from the medial condyle proximally towards the lesser trochanter is a character shared with a plethora of other iguanodontians (Gilmore, 1909; Carpenter & Wilson, 2008), including ~~possibly also~~includinh with SHN.JJS.015 ~~,SHN015 although its preservation hampered the possibility to observe this character,~~ but not with the holotype of *Draconyx loureiroi*. Thus, ~~it~~ ML 434 should be regarded as Ankylopollexia indet based on the pendant 4th trochanter, the base of the 4th trochanter located at the mid-shaft and the scar of M. caudifemoralis longus reaching the base of the 4th trochanter.~~-~~

Phylogenetic analysis

~~The a~~Analysis ~~of the dataset~~ of Bell et al. (2018) dataset returned 99.999 Most Parsimonious Trees ~~MPTs~~ (Consistency~~.~~ I~~.~~ndex = 0.340 R~~.~~etention I~~.~~ndex = 0.638) with length of 920 steps (Fig.11~~9~~). The strict consensus tree lacks ~~enough~~ sufficient resolution for any meaningful discussion, ~~therefore~~ so we identified wildcard taxa using the iterpcr algorithm (Pol & Escapa, 2009), implemented in TNT v1.5. This led to us pruning~~and~~ pruned a posteriori the following taxa: *Atlascopcosaurus*, *Burianosaurus*, *Changchunsaurus*, *Gideonmantellia*, *Haya*, *Laellynasaura*, LRF 50, *Lycorhinus*, *Macrogryposaurus*, *Micropachycephalosaurus*, *Mochlodon vorosi*, *Notohypsilophodon*, *Qantassaurus*, *Stenopelix*, *Thescelosaurus garbani* and *Weewarrasaurus*. The general topology does not differ from the one recovered by the original analysis of Bell *et al*. (2018). ML 357 is recovered within Styracosterna, more deeply nested than *Camptosaurus dispar* in a ~~politomy~~polytomy with ~~alongside~~ *Iguanodon bernissartensis* and *Ouranosaurus nigeriensis*. The inclusion of ML 357 into Styracosterna is based on the presence of a sharply defined cnemial crest (Char. 231:1).

The inclusion of ML 357 into the dataset of Xu et al. (2018) gave consistent results with the previous analysis (Fig.1~~0~~ A), recovering the specimen within ~~Styracosterna~~ ~~as~~Styracosterna as sister to *Dakotadon lakotaensis*, returning a single tree of 311 steps (C.I. =0.627 R.I.=0.893). The general tree topology and the supporting synapomorphies for the nodes of Ankylopollexia and Styracosterna do not differ from the original study of Xu et al. (2018). Styracosterna is supported by the following synapomorphies: a conical mediolaterally enlarged ungu~~e~~al on ~~the~~ manual digit I (Char. 92:1) and ~~by~~ a sub-triangular section of the femoral shaft (Char.116:1). The inclusion of ML 357 in~~to~~ Styracosterna is due to the presence of a splint-like ~~M~~metatarsal I (Char. 121:1). In the present analysis, the genus *Camptosaurus*

as defined by Carpenter and Galton (2018) ~~is~~ was not recovered, therefore it is followed the taxonomic revision of McDonald (2011) and ~~we~~ consider *Uteodon aphanoecetes* and *Cumnoria prestwichii* as distinct genera.

The Bayesian non-clock analysis including ML 357 in Xu *et al*., (2018), found the same tree topology ~~of~~ as the Maximum Parsimony analysis ~~,(~~ see the output maximum compatibility tree (MCT) in fig. 13~~1~~). The ESS value for all parameters is > 200, indicating the good quality and the stationarity phase reached by the analysis. Furthermore, the Potential Scale Reduction Factor (PRSF) is equal to 1 for all parameters, and the Average standard deviation of split frequencies (ASDSF) value is □ 0.004, supporting the interpretation indicated by the ESS values. The marginal likelihood obtained in the Non-Clock analysis is -1381.99 (harmonic mean).

The Clock Analysis, including the topology of the non-Clock analysis implemented as strict prior, obtained parameters ESS values generally >200. In addition, PRSF values for the parameters range from 1.000 to 1.001, and ASDSF value is 0.0000, confirming that convergence and stationarity in our analysis has been achieved. The marginal likelihood obtained in the Clock-Analysis is -1390.60 (harmonic mean).

Evolutionary rates

The analysis (Fig.1~~0~~2 A-C) of the Homoplasy Concentration within the topology obtained by the parsimony analysis of the dataset of Xu et al. (2018) dataset located high rates of homoplasy in various parts of the tree. As evident in this analysis and already pointed out by Rauhut & Pol (2019), homoplasy concentration peaks and evolutionary rates acceleration are directly correlated~~relatable~~ (fig.12~~0~~c-d).The highest peak, as indicated by the XY graphs is at the base of the tree and further back in time. This is because the outgroup, *Lesothosaurus diagnosticus*, is selected as extant by the script in order to calculate

evolutionary rates through time;~~,~~ therefore, this is an artefact produced by the analysis. However, the analysis located two peaks of HC in this topology: the first is at the base of Dryomorpha (Ankylopollexia + Dryosauridae), and the other one is deeply nested within Hadrosauroidea.

The first peak is located approximately between 145 and 135 Ma, comprising the appearance of several basal styracosternan lineages. This shift encompasses the Jurassic-Cretaceous transition, which is generally characterized by peculiar patterns of faunal turnovers and radiations among different groups (Tennant *et al*., 2017). The small inflection at 140 Ma may be due to sampling bias in the fossil record occurring during the earliest s~~S~~tages of Cretaceous (Tennant *et al*., 2017). The second peak, located at approximately around 80 Ma, is related to the appearance of Rhabdodontidae and derived hadrosauroids. High HC rates in the clade Rhabdodontidae, are~~is~~ most probably due to their long ghost lineage, and early divergence~~ing~~ time from the rest of Iguanodontia. The appearance of the high HC rates within Hadrosauroidea is linked to the appearance of more derived Late Cretaceous forms as also noticed by Stubbs et al. (2019), and related increase of morphospace occupation.

The Bayesian inference results do not contradict the ones obtained from ~~by~~ parsimony analysis (Fig.1~~1~~3). The clock analysis revealed acceleration in the evolutionary rates across a wider time range between 170-140 Ma and around 80 Ma, recovering essentially the same signal described above. However, there are slight differences between the results of the two methodologies. First, the time range linked to the radiation of basal styracosternans is essentially longer and 5 Myrs off-set with respect to the previous analysis. This is due to the different ways of Mr.Bayes and TNT script to model age uncertainties, the first modelling this parameter accordingly a uniform distribution while the second creates discrete time-bin (Ronquist *et al*., 2012; Rauhut & Pol, 2019). Second, it does not recover the increase of

evolutionary rates within Rhabdodontidae. On the other hand, it supports the previous analysis in suggesting that the main radiation of basal styracosternans occurred across the Jurassic-Cretaceous transition, and the relative acceleration of evolutionary rates coinciding with derived hadrosauroids.

Length estimation

The application of the fully cursorial model, given the scalar value of 175 mm for metatarsal ~~three~~III, produces a length estimate of 2906 mm, while the sub-cursorial model produces an estimate of 3853 mm. The length ranges, therefore, between 3 and 4 meters. Waskow & Mateus (2017) showed that ML 357 was a senile specimen, approximately 30 years-old. Therefore, our estimation represents the maximum length that the species *Draconyx loureiroi* reached at the end of ~~his~~ its ontogenetic development. This length estimation contrasts with ~~the length of~~ individuals of *Camptosaurus dispar*, *Mantellisaurus atherfieldensis* and *Iguanodon bernissartensis* that reached at the end of their life-histories length up to 7-9 meters (Norman, 1980, 1986; Erickson, 1988). ~~.~~The estimated length for *Draconyx loureiroi* is similar to that ~~e one~~ of *Cumnoria prestwichii*, reported by Galton ~~and~~ & Powell (1980) to be around 4-5 meters; although there is no evidence that the holotype of *C. prestwichii* pertains to a fully mature individual. Therefore, we can consider *Draconyx loureiroi* a relatively small styracosternan species, compared to its close relatives.

Discussion

Systematic position of *Draconyx loureiroi* (ML 357)

~~The type specimen~~ ML 357 has been recovered nested within Styracosterna using both ~~in~~ the Bell *et al*. (2018) and in Xu *et al*. (2018) datasets. Both analyses, as in many cases for the base of Iguanodontia, are not strongly supported. The inclusion of ML 357 within

Styracosterna is ~~alternatively~~ due to the development of the cnemial crest ~~and~~ or the presence of a splint-like m~~M~~etatarsal I, depending the dataset used. In the original description of Mateus & Antunes (2001) a 'vestigial m~~M~~etatarsal I' ~~has been pointed out~~was proposed as possible~~y~~ autapomorphy for this species. However, as pointed out in the comparisons ~~section~~, a reduced metatarsal I is ~~a character~~ common to many styracosternans, although these analyses did not recover it as common synapomorphy for the clade. The development of the cnemial crest in ML 357 is regarded as a synapomorphy for Styracosterna. However, ~~such~~ this character state does not appear to support the inclusion of ML 357 ~~within~~ in other nodes in the matrix~~,~~. The data matrix of Bell et al. (2018) broadly samples Ornithischia, therefore, we consistently consider it diagnostic.

Other characters that support the styracosternan affinities of ML 357 are the fibular condyle of the tibia, which caudally deflected, as also occurs in *Iguanodon bernissartensis*, *Mantellisaurus atherfieldensis* and *Ouranosaurus nigeriensis* (Norman, 1980, 1986; Bertozzo *et al*., 2017). Verdú *et al*. (2018), in his phylogenetic analysis of *Iguanodon galvensis* recovered *Draconyx loureiroi* in an unresolved polytomy within Styracosterna, supporting the present interpretation of ML 357 as styracosternan iguanodontian.

Beside the characters supporting its affinities with Styracosterna, *D. loureiroi* ML 357 possesses a combination of characters ~~, which remark~~ that indicate a complex evolutionary history for iguanodontians. The carpus is not closely packed, as it occurs in dryosaurids and the styracosternan *Uteodon aphanoecetes,* contrasting with the closely packed and interlocked condition of carpal elements in *Camptosaurus dispar* ~~differently from *Camptosaurus dispar*~~ (Fig.1~~2~~4 A-B, D-E, G-H)) ~~that presents closely packed and interlocked carpal elements~~. Further, the carpal bones are not fused as ~~it~~ occurs in derived styracosternans ~~forms~~, such as *Iguanodon bernissartensis*, ~~and~~ *Mantellisaurus atherfieldensis* or *Magnamanus soriaensis* (Fig.1~~2~~4 C, F, I) (Norman, 2004). Generally, the fused condition of

the carpus is associated with the presence of the hypertrophiede conical thumb (spike), which is typical for many Early Cretaceous styracosternans (Norman, 2004). Ankylopollexians, whose hand is known, present unguals just in the first three manual digits (Norman, 1980, 1986; Carpenter & Wilson, 2008), ML 357 presents five out of six unguals for both hands, none of them resembling the morphology of the conical thumb. *Draconyx loureiroi* lacks the hypertrophied conical thumb (spike); instead, it presents possesses a series of claw-like unguals similarly to those of *Uteodon aphanoecetes* and *Camptosaurus dispar.* These data remark highlight the fact there is a close relationship between the close packaging packing of the carpal bones and the presence of the hypertrophied pollex, although they raise the question from which ancestral condition the derived styracosternan carpus arose. The character state that resembles more the possible ancestral condition most is the one present in *Camptosaurus dispar*, as the transition from a rigid interlocked unit to a fused element seems expected. In any cases, *C. dispar* is recovered in a basal position with respect to the clade constituted by *U. aphanoecetes*, and *D. loureiroi* indicating the immediate ancestral condition to the derived Early Cretaceous styracosternans is probably of these two latter forms (Fig.124 A-J). If thisIt is not clear if this result implies a re-evaluation of *C. dispar* species or a deep revision of the characters present in our phylogenetic matrices is not clear at the present time, and this it is beyond the scope of the present contribution.

The hind limb elements also show a mosaic of characters, which singularly are found among several iguanodontian lineages. For instance, the preserved femoral shaft is strongly cranio-caudally bowed, as it occurs in basal ornithopods, dryomorphans and ankylopollexians. Proximally, as in other ankylopollexian species (Gilmore, 1909; Norman, 1980, 1986, 2004), the femur may have a straighter outline although the preservation bias hampers the possibility to properly assess this character. However, the mosaic of characters is most evident in the distal epiphysis: the extensor groove is deep and U-shaped as in

Valdosaurus canaliculatus (Barrett *et al.,* 2011), and ankylopollexians basal to hadrosauriformes. The flexor groove is fully open, ~~presenting not even~~without the slight overhang that is found in some dryosaurid specimens (Galton, 1981), resembling ~~more~~ the condition ~~at the~~in basal ornithopod/neornithischians (Fig.7) (Norman *et al*., 2004).

Furthermore, ~~*Draconyx loureiroi* presents the tibial proximal epiphysis with a concave medial margin~~ the proximal epiphysis of the tibia has a concave medial margin in *Draconyx loureiroi*, as it occurs in elasmarians (Dieudonné *et al*., 2020), while the fibular condyle is in an intermediate position between the one in ~~respect~~ basal ankylopollexian and derived 'iguanodontoid' taxa. In addition, as Dieudonné *et al*., (2020) noted in other L~~l~~aurasian dryomorphans, the short cnemial crest is rounded and sharply defined, and is strongly antero-laterally bowed as the one of other styracosternans (Norman, 1980, 1986, 2004) ~~being strongly antero-laterally bowed~~. This plethora of characters needs further investigation, although it suggests the presence of a signal that may be related to geographical segregation or functional morphology adaptation.

Draconyx loureiroi has a ~~generally~~ gracile pes, compared with other ankylopollexians. The general proportions of metatarsals II-IV are similar to the lightly built species *Cumnoria prestwichii*, *Uteodon aphanoecetes* and *Mantellisaurus atherfieldensis*, differing from the stout and robust condition ~~seen~~ in ~~species such as~~ *Camptosaurus dispar*, ~~or~~ *Iguanodon bernissartensis* and other large-sized styracosternans (Galton & Powell, 1980, Carpenter & Wilson, 2008, Norman, 1980,1986). ~~The m~~Metatarsal I is present and~~-~~ extremely reduced as in *Mantellisaurus atherfieldensis* and other derived styracosternans, differing from dryosaurids and *Camptosaurus dispar* that retain a larger and functional Mt-1 (Gilmore, 1909; Norman, 1980, 1986; Galton, 1981; ~~-~~Norman *et al*., 2004).

Mateus & Antunes (2001) included ~~the species~~ *Draconyx loureiroi* in the clade 'Camptosauridae', then composed ~~by~~ of the species *Camptosaurus dispar*, *C. prestwichii* and

C. depressus. ~~In 2008,~~ Carpenter ~~&~~ ~~and~~ Wilson (2008) ~~-~~instituted the species *Camptosaurus aphanoecetes*, based on the specimens housed~~sted~~ in the Carnegie Museum ~~proceeding~~ recovered from Dinosaur National Monument, Utah. Subsequently, McDonald (2011) ~~in his phylogenetic analysis~~ showed that the genus *Camptosaurus* is paraphyletic, including a set of progressively more deeply nested species, ~~recognizing~~ and he recognized ~~valid~~ the following species as valid: *Camptosaurus dispar*, *Uteodon aphanoecetes*, *Cumnoria prestwichii* and *Osmakasaurus depressus*. However, Carpenter & Lamanna (2015) claimed that *Uteodon aphanoecetes* was based on a chimera, and lumped ~~again~~ the ~~above mentioned~~above-mentioned species back into the genus *Camptosaurus*.

At the present time, the monophyly of ~~the genus~~ *Camptosaurus*, and the clade 'Camptosauridae', as considered by Carpenter & Lamanna (2015) is not supported by phylogenetic analyses (i.e. McDonald, 2011; Verdù *et al*., 2018), ~~,~~including the one presented in this study. Since specimens traditionally assigned to *Camptosaurus* sp. ~~are~~ have been recovered from different stratigraphic intervals, anagenetic processes, such as the ones observed in the Dinosaur Park Formation (Mallon *et al*., 2012; Carr *et al*., 2017; Wilson *et al*., 2020), might have led to the ~~gradually~~ gradual ~~acquiring~~ acquisition of a mosaic of apomorphic and plesiomorphic character states. ~~Before~~ Until there has been a ~~better~~ new assessment of the evolutionary history of iguanodontians in the Morrison Formation, we suggest that it is better to refer to *Camptosaurus* including just the species *C. dispar*.

Tempo and *modo* ~~of~~ ~~evolution~~ of basal iguanodontian dinosaurs evolution

Two different methodologies indicate an increase of evolutionary rates at ~~in~~ two geological moments: the first encompassing the Jurassic-Cretaceous transition, which is related to the origin o~~p~~f several styracosternan~~s~~ lineages, and the second ~~located~~ at around 80 Ma related to the origin of Rhabdodontidae and derived hadrosauroids. Benson *et al*. (2014,

2018) and Stubbs *et al.* (2019) found concordant trends with the ones recovered here. In particular, Benson *et al*. (2014, 2018) in their analyses of body-size evolution through time within Dinosauria located shifts in evolutionary rates of ornithopods in the Late Jurassic and Early Cretaceous at the base of Ankylopollexia, and in the Late Cretaceous at the base of Rhabdodontidae and within the 'eu-hadrosaurian' lineage. Further, Benson *et al*. (2018) stated that 'shifts to larger body size are more frequent than to smaller size in ornithischians' and the evolutionary model that best describes the overall body size evolution in dinosaurs are ~~the~~ Ornstein–Uhlenbeck models. These models describe constrained evolution around macro-evolutionary optima with rare rapid shifts towards different optima (Stanley, 1973; Hansen, 2013). Similarly, Stubbs *et al*. (2019) indicated a shift of evolutionary rates and complex morphospace occupation in Hadrosauroidea.

The first shift in evolutionary rates is the most relevant in terms of its implications for the present contribution. Styracosterna is ~~-~~characterized by generally increased body size ~~respect to more~~in comparison with basal iguanodontians (Norman, 2004). ~~Many characters this clade acquired at some point of its evolution~~The appearance of some evolutionary novelties within this clade (i.e. straight femoral shaft, migration of the 4th trochanter towards the femoral mid-shaft, partially enclosed extensor and flexor grooves, hoof-like manual unguals) are related to this trend (Maidment & Barrett, 2012). Therefore, we consider the shifts recovered by these analyses as the same general trend, and concordant to Ornstein–Uhlenbeck models of evolution, as proposed by Benson *et al*. (2014, 2018). However, we recognize that several lineage-specific transformations may have occurred and diverged by this theoretical general trend, such as lineages at the base of Styracosterna, as discussed below. ~~We remark that~~ Although the findings presented here need further investigation, ~~although~~ the convergence of our and previous analyses is evidenc~~eeing~~ for an interesting interplay of body-size and ~~possibly~~ auto-ecological characters variation in the radiation of

iguanodontian dinosaurs. We hypothesize here that novel characters related to feeding and food processing may have opened the possibility to occupy new ecological niches for iguanodontians, which have resulted consequently into an increase of body size as indicated by Benson *et al*., (2018). This shift resulted into accelerated morphological innovation, producing several adaptations in the skeleton to sustain a semi-quadrupedal stance.

Indicating the ecological and geological drivers of the *tempo* and *modo* that lead to this shift and the following diversity of styracosternans is difficult, since the Jurassic-Cretaceous transition is complex and characterised by various geological events, which lead to faunal turnovers both in marine and terrestrial ecosystems (Tennant *et al*., 2017). The work by Tennant *et al*., (2016, 2017) proposed indicated tectonic activity and eustatic variation across the Jurassic/Cretaceous transition as the primary factors of diversity variation among several tetrapod groups, and this may have influenced the evolutionary rates of those clades crossing passing such through this transition.

Implications for the rise of Styracosterna

Definitive styracosternans appeared no later than the Late Jurassic. The stratigraphic position of ML 357, close to the boundary of Kimmeridgian-Tithonian boundary, makes this specimen one of the oldest representatives of this group (Norman, 2004). *Cumnoria prestwichii* recovered by McDonald (2011) as a styracosternan is Llateower Kimmeridgian in age according the description of Galton & Powell (1980to Benton & Spencer (1995)), while *Uteodon aphanoecetes* is recovered from the lower-middle Tithonian beds of the Brushy Basin Member of the Morrison Formation, being slightly younger than the above-mentioned species (Carpenter & Wilson, 2008). Therefore, despite incomplete and fragmentary *Cumnoria prestwichii* and *Draconyx loureiroi* should closely resemble the basal bauplan of Styracosterna. These two species share a general lightly built skeleton, gracile, and elongate, d

pedal morphology (Galton & Powell, 1980). The small size ~~recovered in this study for~~of *Draconyx ~~loureiroi~~,loureiroi* ~~-~~ is comparable with ~~the ones of~~ *Cumnoria prestwichii*, ~~indicated at~~indicating ~~the dawn of their radiation~~that styracosternans were medium sized animals, smaller than *Camptosaurus dispar* (Carpenter & Galton, 2018). Furthermore, the unfused carpal and manual ungual condition of *Draconyx loureiroi* suggests a different locomotion stance with respect to *Camptosaurus dispar,* which is considered primarily quadrupedal. Maidment & Barrett (2012) supported the interpretation that hoof-like manual unguals are strongly associated ~~to~~ with a quadrupedal stance, as ~~already~~ proposed by Galton (1970) and Norman (1986).

Therefore, the lack of the abovementioned characters~~thereof~~ strongly supports the interpretation of *Draconyx loureiroi* as a bipedal, possibly cursorial, animal inhabiting the forests of Lourinha Formation as indicated by our restoration (Fig. 15). We here propose the hypothesis that Styracosterna arose as a group of relatively small, cursorial animals, which after the Late Jurassic radiated into larger forms, resulting ~~into~~ from accelerated rates of evolution. At the present ~~time~~, since the oldest representatives appear to be European, it is suggested that this clade originated in Europe and eventually dispersed elsewhere. The *tempo* and *modo* of this radiation needs to be better understood, integrating more data points such as palaeogeography. ~~It is here~~We reinforced the hypothesis that more derived iguanodontians appeared in Europe ~~before~~ earlier than previously thought (Castanera *et al*., 2020 a,b; Rotatori *et al*., 2020).

Conclusions

The ornithopod dinosaur *Draconyx loureiroi* ~~has been~~is re-described and re-diagnosed, and new forelimb elements~~elements forelimb have been~~ are here described for the

first time. The holotype and only specimen is ML 357, and previously preferred material is here re-assigned to Ankylopollexia indet. Phylogenetic analysis and anatomical comparisons indicated that *Draconyx loureiroi* can be assigned to Styracosterna. A unique combination of characters unambiguously distinguishes *D. loureiroi* from other species within the clade. The inclusion of *Draconyx loureiroi* within Styracosterna makes it one of the oldest species that can be referred to this clade, suggesting that Europe may have been the ancestral area where Styracosterna originated and from which it later dispersed. The relatively small size of *D. loureiroi*, considered as a senile individual, suggests that basal styracosternans were bipedal and possibly cursorial animals, and later in their evolution, attained larger body sizes and adaptations to quadrupedalism. Analyses of evolutionary rates employing both Maximum Parsimony and Bayesian inference, revealed an increase of evolutionary rates at among basal iguanodontians across the Jurassic/Cretaceous transition, as observed in other tetrapod clades.

Bibliography

Antunes MT, Mateus O. 2003. Dinosaurs of Portugal. *Comptes Rendus Palevol* 2(1): 77–95.

Baron MG. 2019. *Pisanosaurus mertii* and the Triassic ornithischian crisis: could phylogeny offer a solution?. *Historical Biology* 31(8): 967-981.

Barrett PM. 2016. A new specimen of *Valdosaurus canaliculatus* (Ornithopoda: Dryosauridae) from the Lower Cretaceous of the Isle of Wight, England. *Memoirs of Museum Victoria* 74: 29–48. https://doi.org/10.24199/j.mmv.2016.74.04

Barrett PM, Butler RJ, Twitchett RJ, Hutt S. 2011. New material of *Valdosaurus canaliculatus* (Ornithischia: Ornithopoda) from the Lower Cretaceous of southern England. *Special Papers in Palaeontology* 86: 131–163.

Becerra MG, Ramírez MA .2018. Locomotor Morphotypes, Allometry, Linear Regressions and the Smallest Sizes in Ornithischia: Estimating Body Length Using Hind Limb Variables. *Ameghiniana,* 55(5), 491-516.

Bell PR, Herne MC, Brougham, T., Smith ET. 2018. Ornithopod diversity in the Griman Creek Formation (Cenomanian), New South Wales, Australia. *PeerJ* 6: e6008. https://doi.org/10.7717/peerj.6008

Benson RB, Campione NE, Carrano MT., Mannion PD, Sullivan, C, Upchurch, P, Evans DC. 2014. Rates of dinosaur body mass evolution indicate 170 million years of sustained ecological innovation on the avian stem lineage. *PLoS Biol* 12(5): e1001853.

Benson RB, Hunt G, Carrano MT, Campione N. 2018. Cope's rule and the adaptive landscape of dinosaur body size evolution. *Palaeontology*, 61(1): 13-48.

Benton MJ, Spencer PS. 1995. British Late Jurassic fossil reptile sites. In *Fossil Reptiles of Great Britain* 165-214. Springer, Dordrecht.

Bertozzo F, Dalla Vecchia FM, Fabbri, M. 2017. The Venice specimen of *Ouranosaurus nigeriensis* (Dinosauria, Ornithopoda). *PeerJ* 5: e3403.

Boyd CA. 2015. The systematic relationships and biogeographic history of ornithischian dinosaurs. *PeerJ* 3: e1523.

Carpenter K, Galton, PM. 2018. A photo documentation of bipedal ornithischian dinosaurs from the Upper Jurassic Morrison Formation, USA. *Geology of the Intermountain West* 5: 167–207.

Carpenter K., Lamanna MC. 2015. The braincase assigned to the ornithopod dinosaur Uteodon McDonald, 2011, reassigned to Dryosaurus Marsh, 1894: Implications for iguanodontian morphology and taxonomy. *Annals of Carnegie Museum* 83(2): 149–166.

Carpenter K, Wilson Y. 2008. A new species of *Camptosaurus* (Ornithopoda: Dinosauria) from the Morrison Formation (Upper Jurassic) of Dinosaur National Monument, Utah, and a biomechanical analysis of its forelimb. *Annals of Carnegie Museum* 76(4): 227–264.

Carr TD, Varricchio DJ, Sedlmayr JC, Roberts EM, Moore JR. 2017. A new tyrannosaur with evidence for anagenesis and crocodile-like facial sensory system. *Scientific Reports* 7: 44942.

Castanera D, Silva BC, Santos V F, Malafaia E, -Belvedere M. 2020. Tracking Late Jurassic ornithopods in the Lusitanian Basin of Portugal: Ichnotaxonomic implications. *Acta Palaeontologica Polonica* 65(2): 399–412.

Castanera D, Malafaia E, Silva BC, Santos V F, Belvedere, M. 2020. New dinosaur, crocodylomorph and swim tracks from the Late Jurassic of the Lusitanian Basin: implications for ichnodiversity. Lethaia.

Dieudonné PE, Tortosa T, Fernández-Baldor FT, Canudo JI, Díaz-Martínez, I. 2016. An unexpected early rhabdodontid from Europe (Lower Cretaceous of Salas de los Infantes, Burgos Province, Spain) and a

re-examination of basal iguanodontian relationships. *PloS one* 11(6): e0156251.

Dieudonné PE, Cruzado-Caballero P, Godefroit P, Tortosa T. 2020. A new phylogeny of cerapodan dinosaurs. *Historical Biology* 0(0): 1–21. https://doi.org/10.1080/08912963.2020.1793979

Dodson P. 1980. Comparative osteology of the American ornithopods *Camptosaurus* and *Tenontosaurus*. *Memoirs of the Society of Geology, France*, *139*, 81–85.

Escaso F, Ortega F, Dantas P, Malafaia E, Silva BC, Gasulla JM, Mocho P, Narváez I., Sanz JL. 2014. A new dryosaurid ornithopod (Dinosauria, Ornithischia) from the Late Jurassic of Portugal. *Journal of Vertebrate Paleontology* 34(5): 1102–1112. https://doi.org/10.1080/02724634.2014.849715

Erickson BR. 1988. Notes on the postcranium of *Camptosaurus*. *Scientific Publications of the Science Museum of Minnesota,* 6-13.

Forster CA. 1990. The postcranial skeleton of the ornithopod dinosaur *Tenontosaurus tilletti*. *Journal of Vertebrate Paleontology*, 10(3): 273-294.

Foster J. (2020). *Jurassic West: The Dinosaurs of the Morrison Formation and Their World* (Second Edition). Indiana University Press.

Galton PM. 1970. The posture of hadrosaurian dinosaurs. *Journal of Paleontology*, 464–473.

Galton PM. 1974. *The ornithischian dinosaur Hypsilophodon from the Wealden of the Isle of Wight*. London : British Museum (Natural History). https://trove.nla.gov.au/version/12761293

Galton PM .1980a. European Jurassic ornithopod dinosaurs of the families Hypsilophodontidae and Camptosauridae. *Neues Jahrbuch für Geologie und Paläontologie, Abhandlungen*, 160(1): 73–95.

Galton PM. 1980b. Partial skeleton of *Dracopelta zbyszewskii* n. Gen. and n. Sp., an ankylosaurian dinosaur from the Upper Jurassic of Portugal. *Géobios* 13(3): 451–457.

Galton PM. 1981. *Dryosaurus*, a hypsilophodontid dinosaur from the Upper Jurassic of North America and Africa postcranial skeleton. *Paläontologische Zeitschrift*, 55(3–4): 271–312.

Galton PM. 1983. The cranial anatomy of *Dryosaurus*, a hypsilophodontid dinosaur from the Upper Jurassic of North America and East Africa, with a review of hypsilophodontids from the Upper Jurassic of North America. *Geologica et Palaeontologica* 17: 207–243.

Galton PM. 2006. Teeth of ornithischian dinosaurs (mostly Ornithopoda) from the Morrison Formation (Upper Jurassic) of Western United States. *Horns and Beaks. Ceratopsian and Ornithopod Dinosaurs. Indiana University Press, Bloomington*, 17–47.

Galton PM. 2009. Notes on Neocomian (Lower Cretaceous) ornithopod dinosaurs from England—

Hypsilophodon, Valdosaurus, "Camptosaurus", "Iguanodon"— and referred specimens from Romania and elsewhere. *Revue de Paléobiologie* 28: 211–273.

Galton PM, Powell HP. 1980. The ornithischian dinosaur *Camptosaurus prestwichii* from the Upper Jurassic of England. *Palaeontology* 23(2): 411–443.

Gilmore CW. 1909. Osteology of the Jurassic reptile *Camptosaurus*: with a revision of the species of the genus, and description of two new species. *Proceedings of the United States National Museum* 36: 197–332.

Goloboff, PA, Catalano SA .2016. TNT version 1.5, including a full implementation of phylogenetic morphometrics. *Cladistics* 32: 221–238.

Hansen TF. 2013. Adaptive landscapes and macroevolutionary dynamics. In: Svensson, E., Calsbeek, R. (Eds.). *The adaptive landscape in evolutionary biology*, 205-26. Oxford University Press.

Heath, TA, Huelsenbeck JP, Stadler T.2014. The fossilized birth–death process for coherent calibration of divergence-time estimates. *Proceedings of the National Academy of Sciences* 111(29), E2957-E2966.

Herne MC, Nair JP, Evans AR, Tait AM. 2019. New small-bodied ornithopods (Dinosauria, Neornithischia) from the Early Cretaceous Wonthaggi Formation (Strzelecki Group) of the Australian-Antarctic rift system, with revision of *Qantassaurus intrepidus* Rich and Vickers-Rich, 1999. *Journal of Paleontology*, 93(3): 1–42.

Hess R. 2010. *Blender Foundations: The Essential Guide to Learning Blender 2.6*. Focal Press.

Hill G. 1989. Distal alluvial fan sediments from the Upper Jurassic of Portugal: Controls on their cyclicity and channel formation. *Journal of the Geological Society* 146(3): 539–555.

Ibiricu LM, Casal GA, Martínez RD, Luna M, Canale JI, Álvarez BN, González Riga B. 2019. A new ornithopod dinosaur (Dinosauria: Ornithischia) from the Late Cretaceous of central Patagonia. *Cretaceous Research* 98: 276–291. https://doi.org/10.1016/j.cretres.2019.02.001

Kullberg JC, da Rocha RB, Soares AF., Duarte, LV, Marques, JF. 2014. Palaeogeographical evolution of the Lusitanian Basin (Portugal) during the Jurassic. Part I: The tectonic constraints and sedimentary response. *STRATI 2013* 665–672.

Lewis PO. 2001. A likelihood approach to estimating phylogeny from discrete morphological character data. *Systematic biology* 50(6): 913-925.

Madzia D, Boyd CA, Mazuch M. 2018. A basal ornithopod dinosaur from the Cenomanian of the Czech Republic. *Journal of Systematic Palaeontology* 16(11): 967–979. https://doi.org/10.1080/14772019.2017.1371258

Maidment, SC, Barrett PM. 2012. Osteological correlates for quadrupedality in ornithischian dinosaurs. *Acta Palaeontologica Polonica* 59(1): 53–70.

Mallon JC, Evans DC, Ryan MJ, Anderson JS. 2012. Megaherbivorous dinosaur turnover in the Dinosaur Park Formation (upper Campanian) of Alberta, Canada. *Palaeogeography, Palaeoclimatology, Palaeoecology* 350:124–138.

Mantell GA. 1825. Notice on the *Iguanodon*, a newly discovered fossil reptile, from the sandstone of Tilgate Forest, in Sussex. *Phil. Trans. Roy. Soc.* London 115: 179–186.

Marsh OC. 1881. Principal characters of American Jurassic dinosaurs. Part V. *American Journal of Science (Series 3)* 21: 417–423.

Mateus O, Antunes MT. 2001. *Draconyx loureiroi*, a new camptosauridae (Dinosauria, Ornithopoda) from the Late Jurassic of Lourinhã, Portugal. *Annales de Paléontologie* 87(1): 61–73. https://doi.org/10.1016/S0753-3969(01)88003-4

~~Mateus O, Maidment, SC, Christiansen NA. 2009. A new long-necked 'sauropod-mimic' stegosaur and the evolution of the plated dinosaurs. *Proceedings of the Royal Society B: Biological Sciences* 276(1663): 1815–1821.~~

Mateus O, Dinis J, Cunha, PP. 2017. The Lourinhã Formation: The Upper Jurassic to lower most Cretaceous of the Lusitanian Basin, Portugal – landscapes where dinosaurs walked. *Ciências Da Terra - Earth Sciences Journal* 19(1): 75–97. https://doi.org/10.21695/cterra/esj.v19i1.355

McDonald AT. 2011. The taxonomy of species assigned to *Camptosaurus* (Dinosauria: Ornithopoda). *Zootaxa* 2783(1): 52–68. https://doi.org/10.11646/zootaxa.2783.1.4

McDonald AT. 2012. Phylogeny of Basal Iguanodonts (Dinosauria: Ornithischia): An Update. *Plos One* 7(5), e36745. https://doi.org/10.1371/journal.pone.0036745

McDonald AT, Espílez E, Mampel L, Kirkland JI, Alcalá L. 2012. An unusual new basal iguanodont (Dinosauria: Ornithopoda) from the Lower Cretaceous of Teruel, Spain. *Zootaxa,* 3595: 61-76. https://doi.org/10.11646/ZOOTAXA.3595.1.3

Milner AR, Norman DB. 1984. The biogeography of advanced ornithopod dinosaurs (Archosauria: Ornithischia)—a cladistic-vicariance model. In: E. Reif and F. Westphal (eds.), *Third Symposium on Mesozoic Terrestrial Ecosystems, Short Papers*, 145–150. Attempto Verlag, Tubingen

Norman DB. 1980. On the ornithischian dinosaur Iguanodon bernissartensis from the lower Lower Cretaceous of Bernissart (Belgium). *Memoir de l'Institut Royal des Sciences Naturelles de Belgique*, *178*, 1–105.

Norman DB. 1986. On the anatomy of *Iguanodon atherfieldensis* (Ornithischia: Ornithopoda). *Bulletin de l'Institut royal des Sciences naturelles de Belgique* 56: 281–372.

Norman DB. 2004. Basal iguanodontia. In: Weishampel DB, Dodson P, Osmolska H, eds. *The Dinosauria*. Berkeley: University of California, 413–437.

Norman DB, Sues HD, Witmer, LM, Coria RA 2004. Basal ornithopoda. In: Weishampel DB, Dodson P, Osmolska H, eds. *The Dinosauria* 393–412.

Norman DB. 2011. On the osteology of the lower Wealden (Valanginian) ornithopod *Barilium dawsoni* (Iguanodontia: Styracosterna). *Special Papers in Palaeontology* 86: 165–194.

Norman DB. 2015. On the history, osteology, and systematic position of the Wealden (Hastings group) dinosaur *Hypselospinus fittoni* (Iguanodontia: Styracosterna). *Zoological Journal of the Linnean Society* 173(1): 92–189.

Owen~~,~~ R. 1842. Report on British fossil reptiles. Part II. In: *Report of the Eleventh Meeting of the British Association for the Advancement of Science*, Plymouth, England, July 1841, 60–204. John Murray, London.

Pol~~,~~ D, ~~D., &~ Escapa~~,~~ I.~~-~~H. 2009. Unstable taxa in cladistic analysis: identification and the assessment of relevant characters. *Cladistics*, 25(5), 515-527.

Rambaut A, Drummond A J, Xie D, Baele, G, Suchard, MA. (2018). Posterior summarization in Bayesian phylogenetics using Tracer 1.7. *Systematic biology* 67(5), 901.

Rauhut OW, Pol D. 2019. Probable basal allosauroid from the early Middle Jurassic Cañadón Asfalto Formation of Argentina highlights phylogenetic uncertainty in tetanuran theropod dinosaurs. *Scientific reports* 9(1): 1-9.

Ronquist F, Teslenko M., Van Der Mark P, Ayres DL, Darling A, Höhna S, Larget B, Liu L, Suchard MA, Huelsenbeck, JP. (2012). MrBayes 3.2: efficient Bayesian phylogenetic inference and model choice across a large model space. *Systematic biology* 61(3): 539-542.

Rotatori FM, Moreno-Azanza M, Mateus O. 2020. New information on ornithopod dinosaurs from the Late Jurassic of Portugal. *Acta Palaeontologica Polonica* 65(1): 35–57.

Rozadilla S, Agnolín FL, Novas FE. 2019. Osteology of the Patagonian ornithopod *Talenkauen santacrucensis* (Dinosauria, Ornithischia). *Journal of Systematic Palaeontology* 0(0): 1–47. https://doi.org/10.1080/14772019.2019.1582562

Rozadilla S, Cruzado-Caballero P, Calvo JO. 2020. Osteology of Ornithopod *Macrogryphosaurus gondwanicus* (Dinosauria, Ornithischia) from the Upper Cretaceous of Patagonia, Argentina. *Cretaceous Research* 108: 104311.

Ruiz-Omeñaca JI, Pereda Suberbiola X, Galton PM. 2006. *Callovosaurus leedsi*, the earliest dryosaurid dinosaur (Ornithischia: Euornithopoda) from the Middle Jurassic of England. In: K. Carpeneter (ed.), *Horns and Beaks: Ceratopsian and Ornithopod Dinosaurs*, 3–16. Indiana University Press, Bloomington.

Seeley HG. 1887. On the classification of the fossil animals commonly called Dinosauria. *Proceedings of the Royal Society of London* 43: 165–17.

Sereno, PC. 1986. Phylogeny of the bird-hipped dinosaurs (Order Ornithischia). *National Geographic Research* 2: 234–256.

Simões TR, Vernygora O., Caldwell MW, Pierce SE. (2020). Megaevolutionary dynamics and the timing of evolutionary innovation in reptiles. *Nature communications* 11(1): 1-14.

Simões TR, Caldwell MW, Pierce SE. (2020). Sphenodontian phylogeny and the impact of model choice in Bayesian morphological clock estimates of divergence times and evolutionary rates. *BMC biology* 18(1): 1-30.

Stanley SM .1973. An explanation for Cope's rule. *Evolution* 27: 1-26.

Stubbs TL, Benton MJ, Elsler A., Prieto-Márquez A. 2019. Morphological innovation and the evolution of hadrosaurid dinosaurs. *Paleobiology* 45(2): 347-362.

Tennant JP, Mannion, PD, Upchurch P .2016. Sea level regulated tetrapod diversity dynamics through the Jurassic/Cretaceous interval. *Nature Communications* 7(1), 1-11.

Tennant JP, Mannion, PD, Upchurch P, Sutton MD, Price GD. 2017. Biotic and environmental dynamics through the Late Jurassic–Early Cretaceous transition: evidence for protracted faunal and ecological turnover. *Biological Reviews* 92(2): 776-814.

Taylor AM, Gowland S, Leary S, Keogh KJ, Martinius AW. 2014. Stratigraphical correlation of the Late Jurassic Lourinhã Formation in the Consolação Sub-basin (Lusitanian Basin), Portugal. *Geological Journal* 49(2): 143–162. https://doi.org/10.1002/gj.2505

Verdú FJ, Cobos A, Royo-Torres R, Alcalá L. 2019. Diversity of large ornithopod dinosaurs in the upper Hauterivian-lower Barremian (Lower Cretaceous) of Teruel (Spain): A morphometric approach. *Spanish Journal of Palaeontology* 34(2): 269–288.

Verdú FJ, Royo-Torres R, Cobos A, Alcalá L .2018. New systematic and phylogenetic data about the early Barremian Iguanodon galvensis (Ornithopoda: Iguanodontoidea) from Spain. *Historical Biology* 30(4): 437–474.

Vidarte, C. F., Calvo, M. M., Fuentes, F. M., & Fuentes, M. M. (2016). Un nuevo dinosaurio estiracosterno (Ornithopoda: Ankylopollexia) del Cretácico Inferior de España. Spanish Journal of Palaeontology, 31(2), 407-446.

Waskow K, Mateus O. 2017. Dorsal rib histology of dinosaurs and a crocodylomorph from western Portugal: Skeletochronological implications on age determination and life history traits. *Comptes Rendus Palevol* 16(4): 425–439. https://doi.org/10.1016/j.crpv.2017.01.003

Wilson JP, Ryan MJ, Evans DC. 2020. A new, transitional centrosaurine ceratopsid from the Upper Cretaceous Two Medicine Formation of Montana and the evolution of the '*Styracosaurus*-line'dinosaurs. *Royal Society Open Science* 7(4): 200284.

Winkler DA, Murry PA, Jacobs LL. (1997). A new species of *Tenontosaurus* (Dinosauria: Ornithopoda) from the Early Cretaceous of Texas. *Journal of Vertebrate Paleontology* 17(2) 330-348.

Xu X, Tan Q, Gao Y, Bao Z, Yin Z, Guo B, Wang J, Tan L, Zhang Y, Xing H. 2018. A large-sized basal ankylopollexian from East Asia, shedding light on early biogeographic history of Iguanodontia. *Science Bulletin* 63(9): 556–563. https://doi.org/10.1016/j.scib.2018.03.016

SUPPORTING INFORMATION

Supplementary 1: data matrix of Madzia et al., 2018 implementing Bell et al., 2018 modifications, including ML 357

Supplementary 2: data matrix of Xu et al., 2018 implementing including ML 357

Supplementary 3: Nexus infile of the NonClock Analysis

Supplementary 4: Nexus infile of the Clock Analysis

Supplementary 5: 3D File of the articulated leg of *Draconyx loureiroi* holotype, ML357

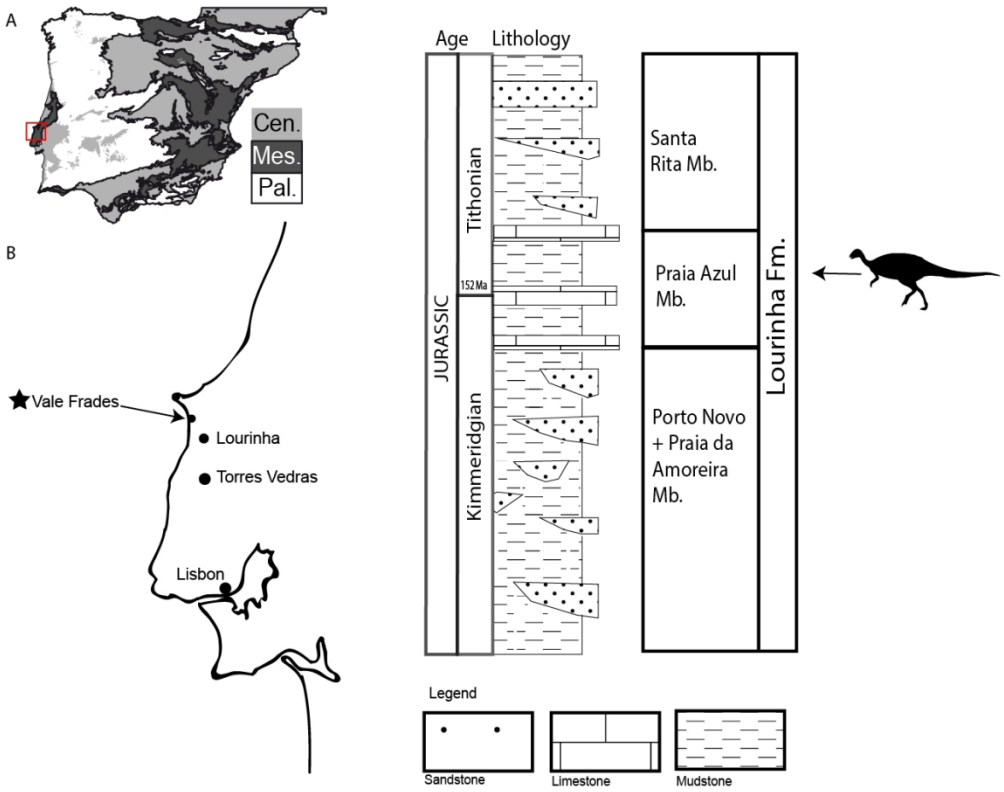

Fig.1. Geographical and geological settings of ML 357. Stratigraphic log of the Lourinhã Formation and position of the specimen. Re-adapted from Rotatori et al., 2020. Map of Iberian Peninsula courtesy of Eduardo Puertolas-Pascual.

111x124mm (300 x 300 DPI)

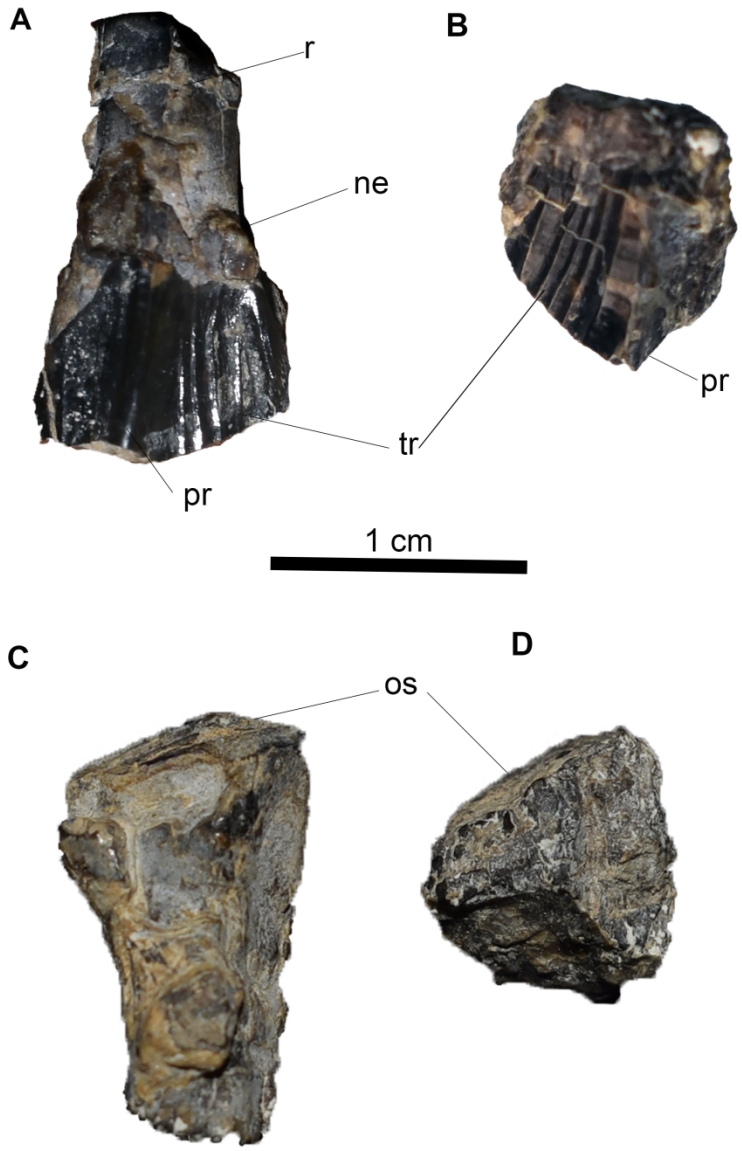

Fig.2. two maxillary teeth of ML 357 in labial and lingual views. Completely preserved maxillary in labial (A) and lingual (C) views; isolated maxillary crown in labial (B) and lingual (D) views. Abbreviations: ne: neck, os: occlusal surface, pr: primary ridge, tr: tertiary ridges.

912x1315mm (72 x 72 DPI)

Fig.3. general overview of ML 357 post-cranial skeleton. Caudal vertebrae (K-M) in left lateral view. Right femur (A-E) in (A) frontal, (B) medial, (C) caudal, (D) lateral and (E) distal views. Right tibia in medial (F) and (G) lateral views. Proximal end of the fibula in medial (I) and lateral (J) views. Right articulated pes in dorsal (N) and medial view (Q). Pedal digit III (O) and pedal digit II (P) in dorsal view.

1399x1874mm (72 x 72 DPI)

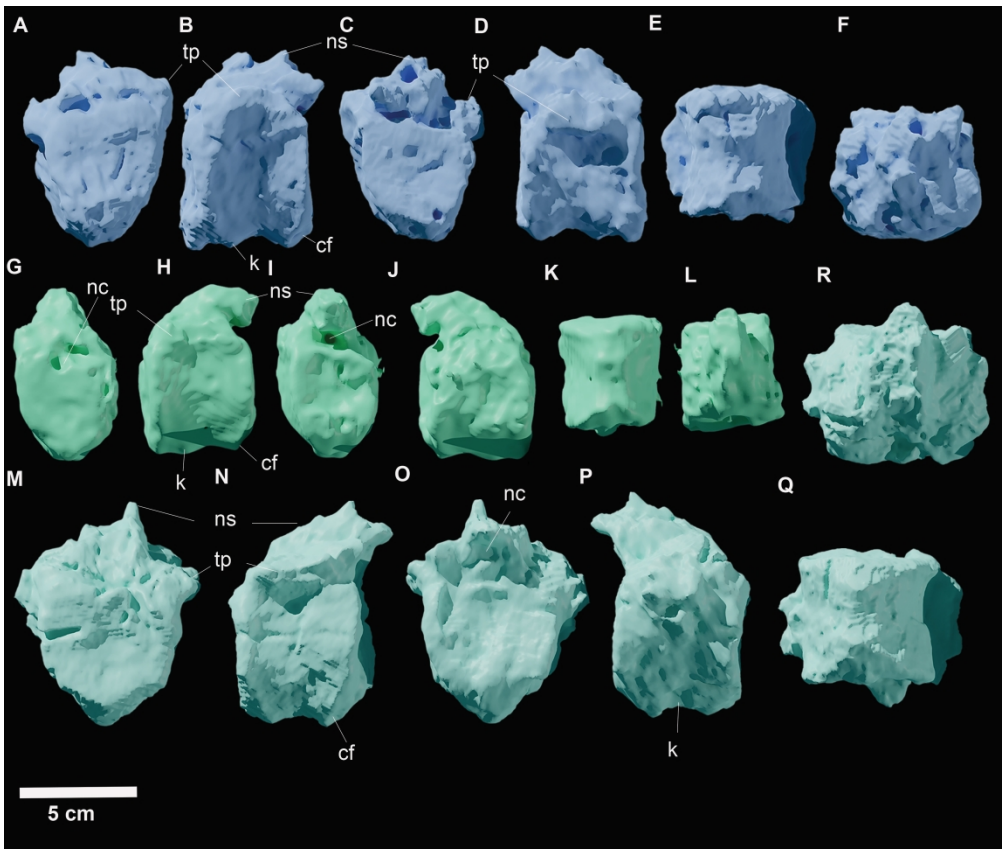

Fig.4. Three dimensional models of axial skeleton of ML 357. (A-F): Caudal n.2 ML 357-10 in (A) cranial view, (B) left lateral view, (C) caudal view, (D) right lateral view, (E) ventral view and (F) dorsal view. Caudal n.3 ML 357-11 (G-L) (G) cranial view, (H) left lateral view, (I) caudal view, (J) right lateral view, (K) ventral view and (L) dorsal view. Caudal n.1 ML 357-9(M-R): (M) cranial view, (N) left lateral view, (O) caudal view, (P) right lateral view, (Q) ventral view and (R) dorsal view. Abbreviations: cf: chevron facet, k: keel, nc: neural canal, ns: neural spine, tp: transverse process.

1399x1180mm (72 x 72 DPI)

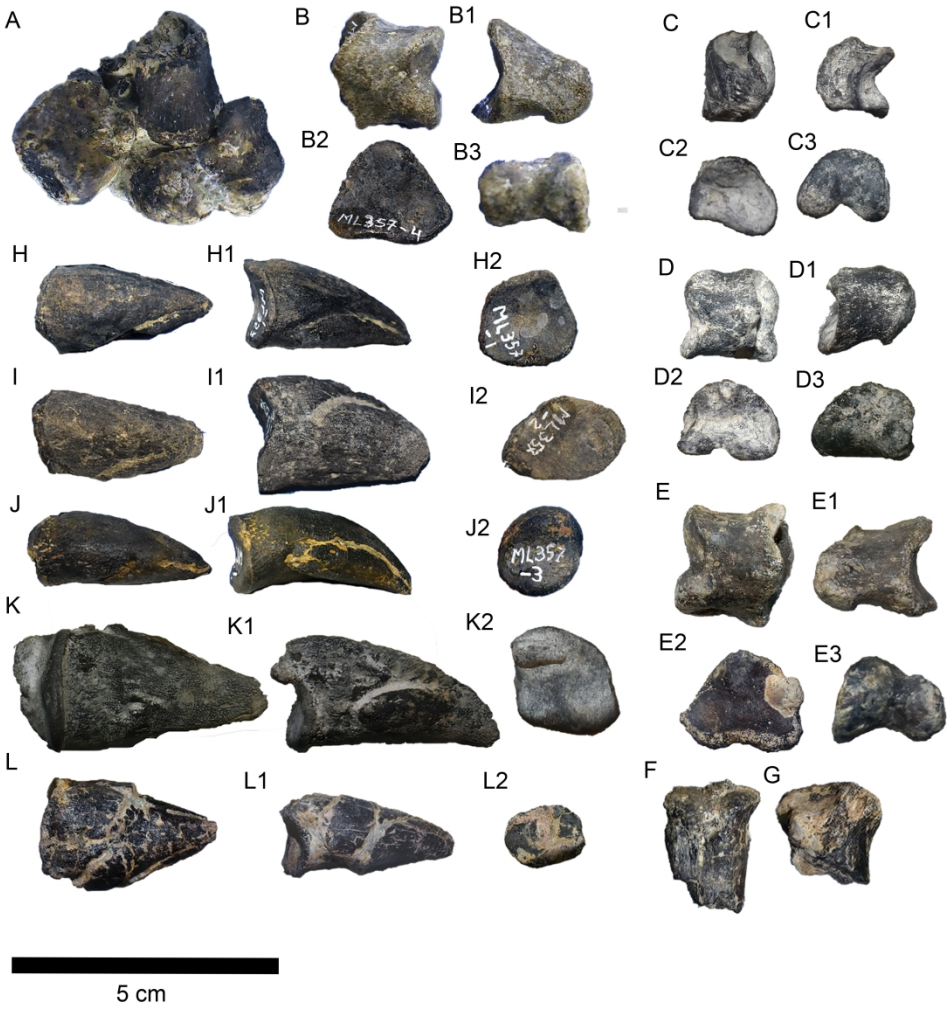

Fig.5. Manual elements of ML 357 (ML 357 1-5, 20-26), including articulated partial carpus, manual phalanges and unguals (A- L). Articulated partial carpus (ML 357 – 5) in extensor view (A), right phalanx n.1(ML 357 – 4) in dorsal view (B), lateral view (B1), proximal view (B2) and distal view (B3), left phalanx n.2 (ML 357 – 22) in dorsal view (C), lateral view (C 1), proximal view (C2) and distal view (C3), left phalanx n.3 (ML 357 – 21) in dorsal view (D), lateral view (D1), proximal view (D2) and distal view (D3), left phalanx n.4 (ML 357 – 24) in dorsal view (E), lateral view (E1), proximal view (E2) and distal view (E3), isolated distal ends of tarsals (ML 357 – 25,26) in extensor view (F,G), left ungual phalanx n.1 in dorsal view (D), medio-lateral view (D1) and proximal view (D2), left ungual phalanx n.1 (ML 357-1) in dorsal view (H), medio-lateral view (H1) and proximal view (H2), right ungual phalanx n.2 (ML 357 – 2) in dorsal view (I), medio-lateral view (I1) and proximal view (I2), right ungual phalanx n.3 (ML 357 – 3) in dorsal view (J), medio-lateral view (J1) and proximal view (J 2), left ungual phalanx n.4 in dorsal view (K), medio-lateral view (K1) and proximal view (K2), ungual phalanx n.5 (ML 357 – 20) in dorsal view (L), medio-lateral view (L1) and proximal view (L2).

1264x1296mm (72 x 72 DPI)

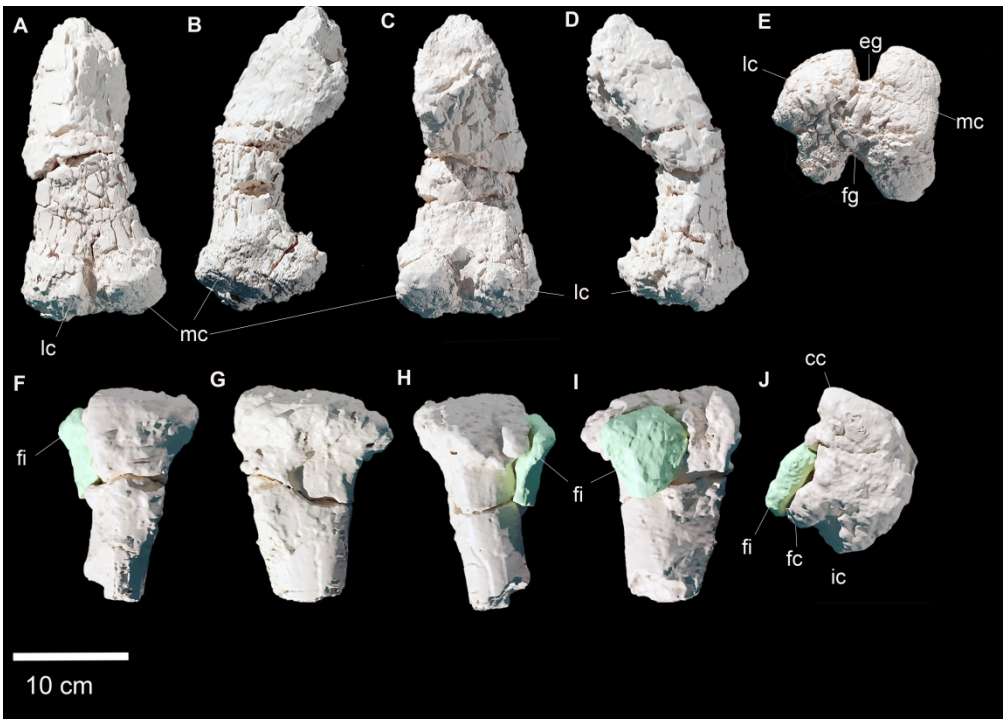

Fig.6. Three dimensional models of limb bones elements of ML 357(ML 357 6-8), femur (A-E) and tibia and proximal end of fibula (F-J). Femur (ML 357 – 6) in (A) cranial view, (B) medial view, (C) caudal view, (D) lateral view and (E) distal view. Tibia (ML 357 – 7) and proximal end of fibula (ML 357 – 8) in (F) cranial view, (G) medial view, (H) caudal view, (I) lateral and (E) proximal view.

1399x997mm (72 x 72 DPI)

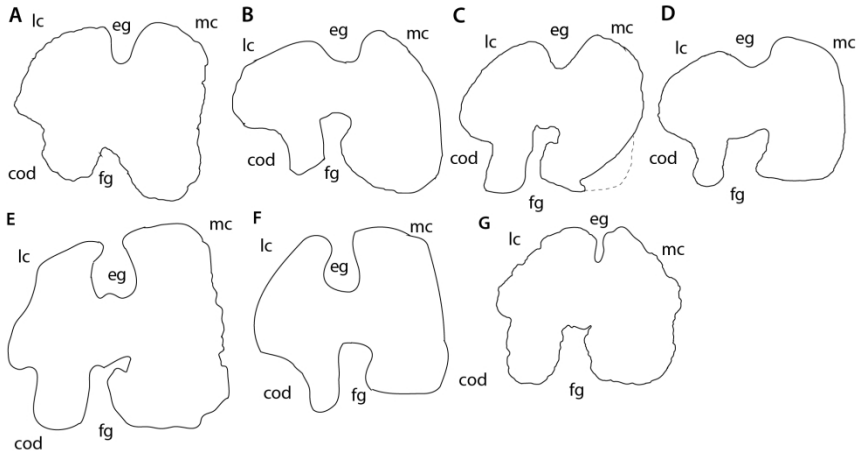

Fig.7 Comparative table of distal sections of femoral shaft from selected iguanodontians. (A) *Draconyx loureiroi*, (B) *Uteodon aphanoecetes*, (C) *Cumnoria prestwichii* , (D) *Camptosaurus dispar*, (E) *Barilium dawsoni* , (F) *Mantellisaurus atherfieldensis* and (G) *Iguanodon galvensis* . Abbreviations: cod: condylid, eg: extensor groove, fg: flexor groove, lc: lateral condyle, mc: medial condyle. Distal sections drawn from: Carpenter & Wilson, 2008; Galton & Powell, 1981; Norman, 2011; Norman, 1986; Verdù et al., 2017.

194x95mm (300 x 300 DPI)

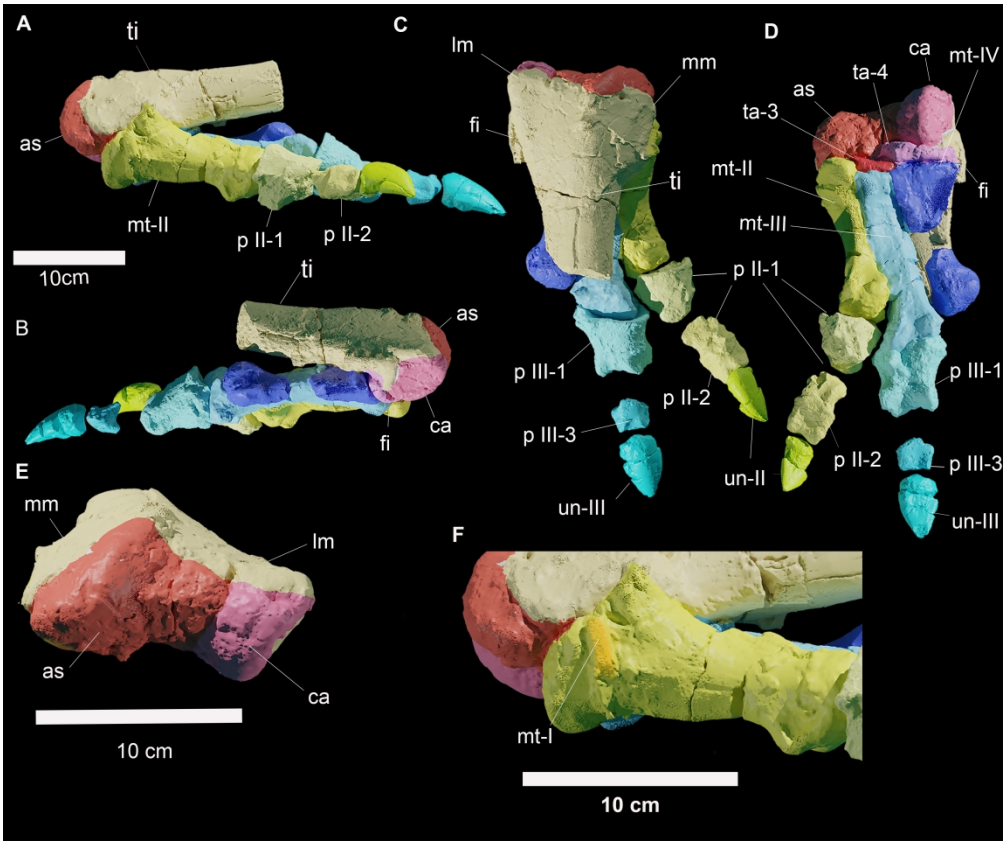

Fig.8. Three dimensional models of the pes of ML 357. Articulated pes (ML 357-12) (A-E) in (A) medial, (B) lateral, (C) dorsal, (D) plantar view and (E) caudal view. (E) detail of Metatarsal I. Abbreviations: as: astragalus, ca, calcalneum, fi: fibula, lm: lateral malleolus, mm: medial malleolus, mt-I: metatarsal I, mt-II: metatarsal II, mt-III: metatarsal III, mt-IV: metatarsal IV, p II-1: pedal phalanx II-1, p II-1: pedal phalanx II-2, p III-1: pedal phalanx III-1, p III-3: pedal phalanx III-3, ta-3: tarsal 3, ta-4: tarsal 4, un-II: ungual II, un-III: ungual III.

1399x1171mm (72 x 72 DPI)

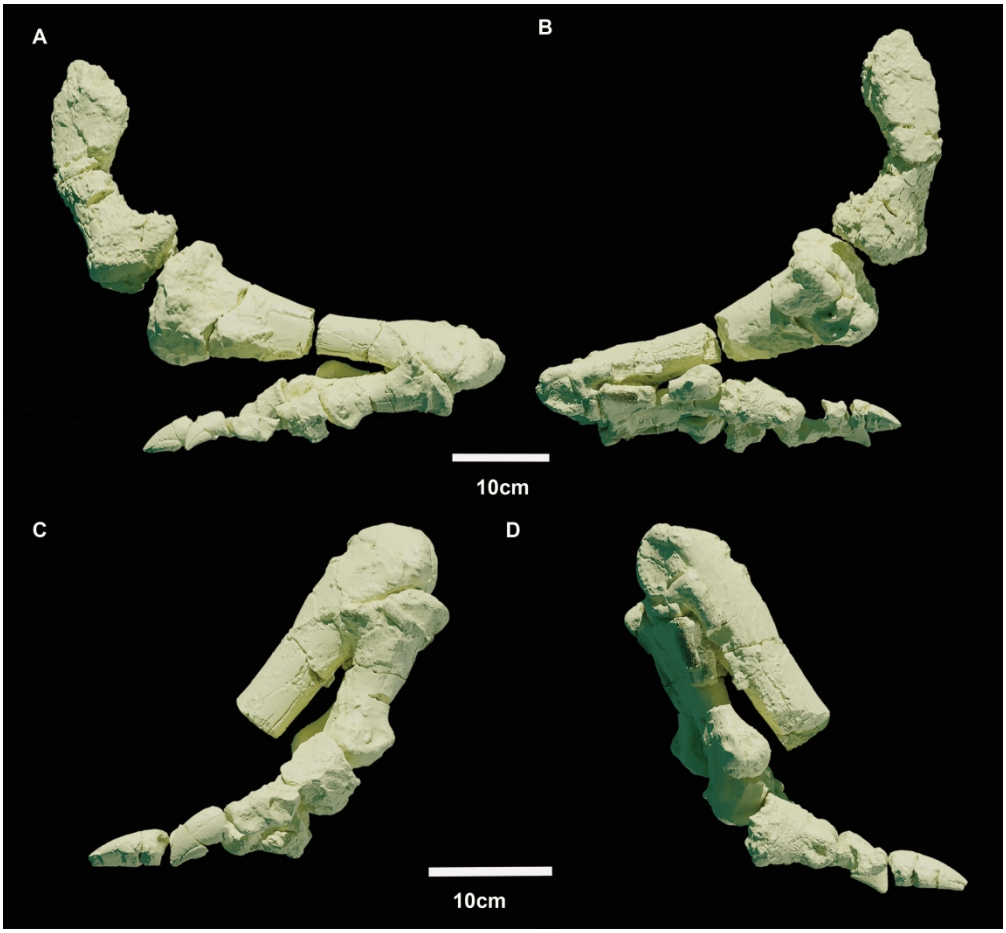

Fig.9. Three dimensional models of the articulated leg (A-B) and pes (C-D) of ML 357. Leg in (A) medial view and (B) lateral view. Pes in (C) medial and (D) lateral view.

1399x1296mm (72 x 72 DPI)

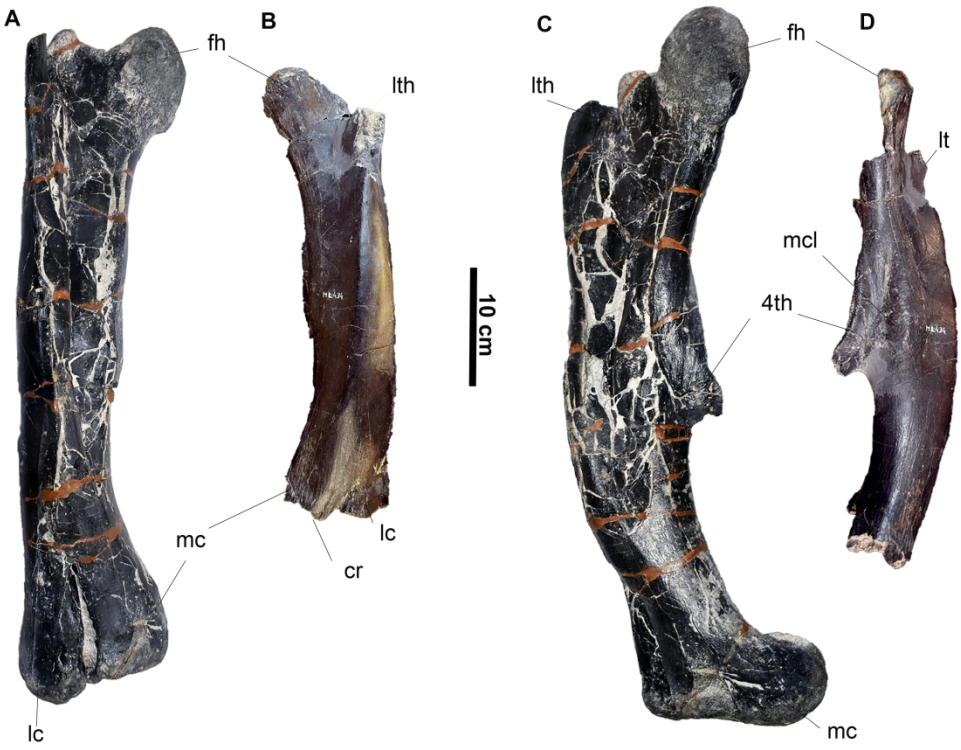

Fig.10. Comparative table between the left femur ML 434 and the right femur SHN.015LPP. Femur SHN.015 and ML 434 in cranial (A, C) and medial (B, D) view. Abbreviations: 4th: fourth trochanter, cr, crest, fh, femoral head, lc, lateral condyle, lt, lesser trochanter, mc, medial condyle, mcl, scar of the Musculus caudifemoralis longus.

1303x1030mm (72 x 72 DPI)

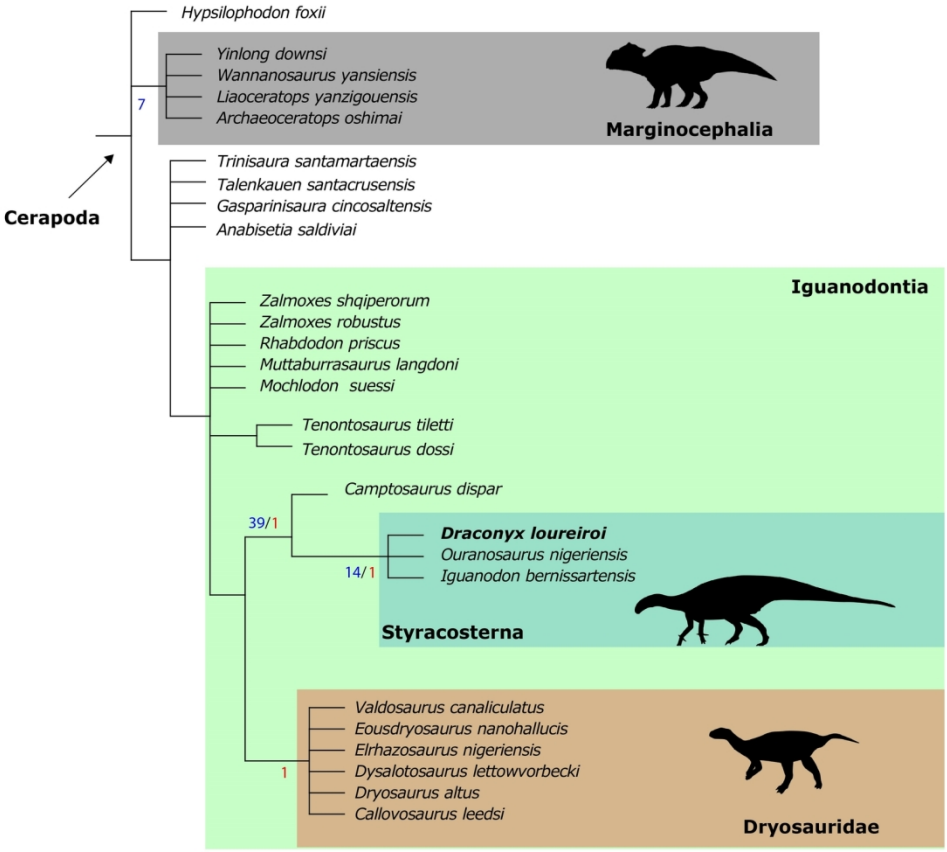

Fig.11. Pruned strict consensus tree of the parsimony analysis of the dataset of Bell et al. (2018). Bootstrap value in blue, Bremer support in red.. Silhouettes from phylopic.org. Credit to: Nobu Tamyra, Matthew Dempsey and Gareth Monger.

153x131mm (300 x 300 DPI)

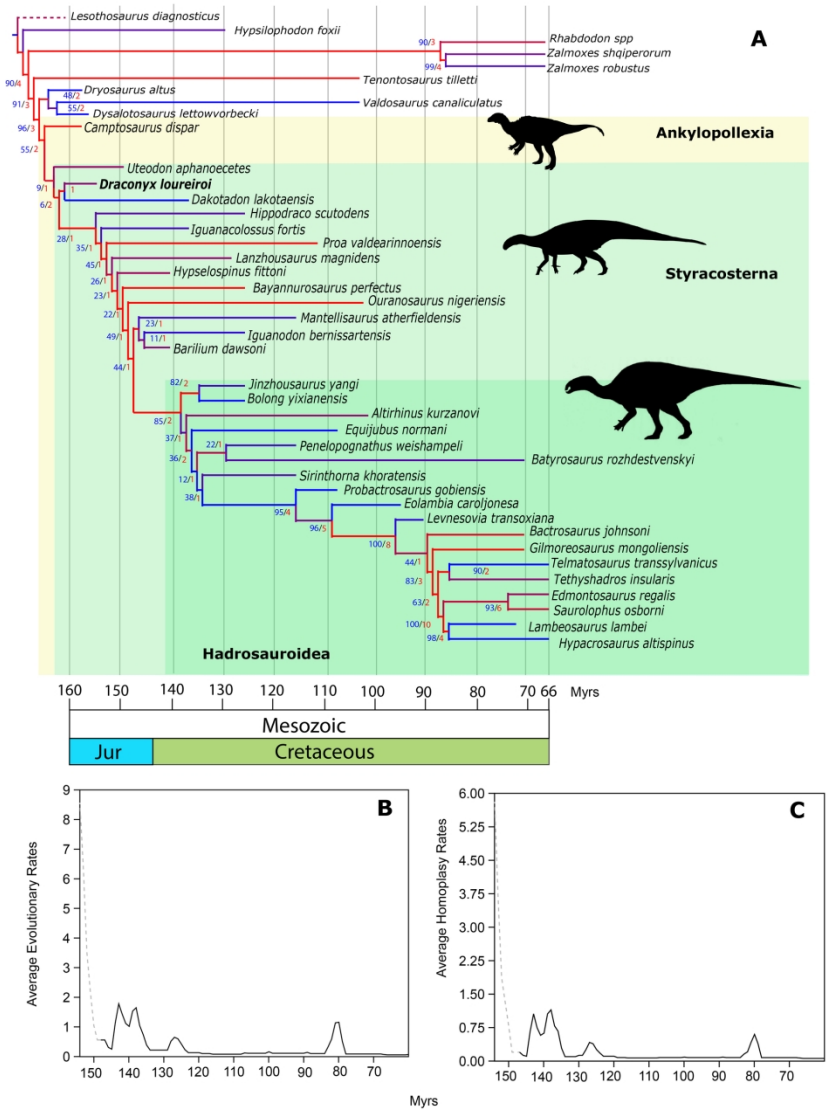

Fig.12. Time calibrated strict consensus tree of the analysis including *Draconyx loureiroi* in the dataset of Xu et al. (2018) (A). Bootstrap value in blue, Bremer support in red. Red colour is associated to increasing of Homoplasy Concentration index. XY graphs of Average Evolutionary Rates (B) and Average Homoplasy Rates (C) through time. Note the coinciding peaks of both AER and AHR. Silhouettes from phylopic.org. Credit to: Michael Keesey, Matthew Dempsey and Pete Buchholz.

161x235mm (300 x 300 DPI)

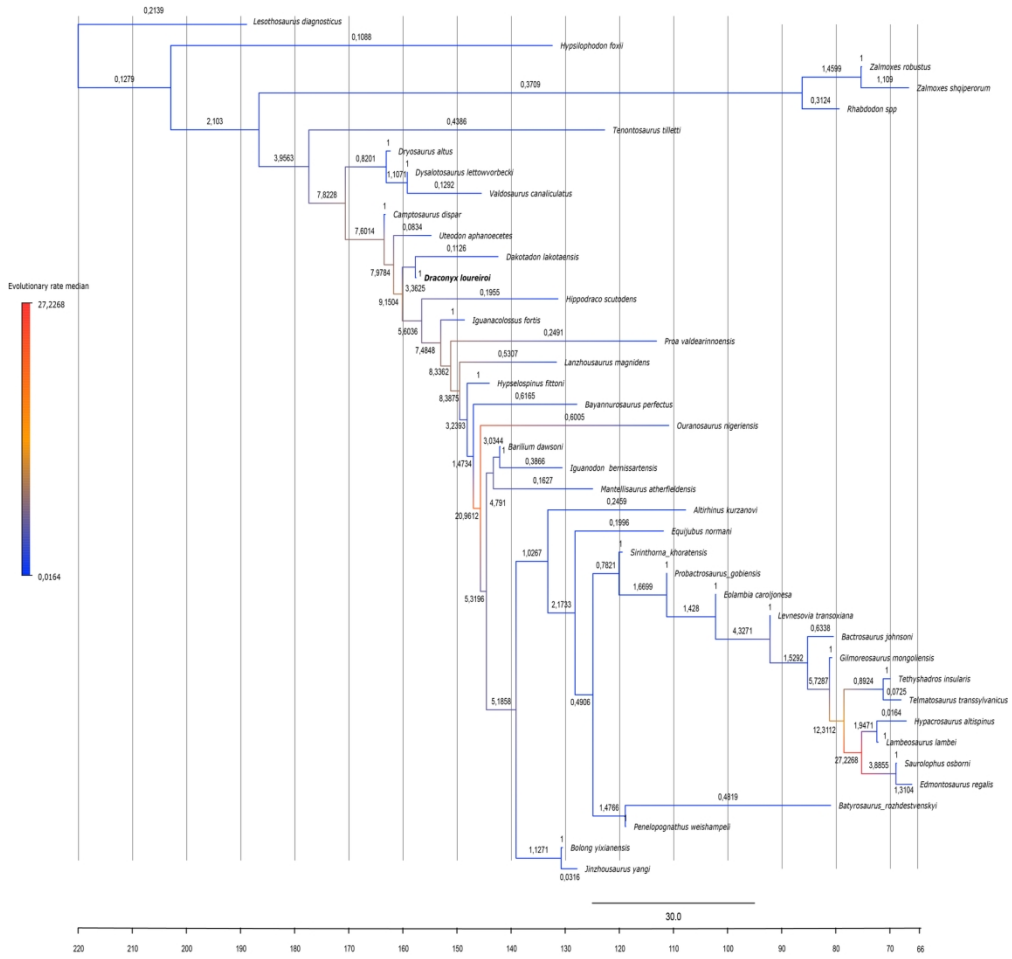

Fig.13. Time calibrated Maximum Compatibility Tree (MCT) of the Bayesian clock analysis of the dataset of Xu et al. (2018). Colours of the branches reflect median of the Evolutionary rates and number represents their absolute values along branches themselves.

165x157mm (300 x 300 DPI)

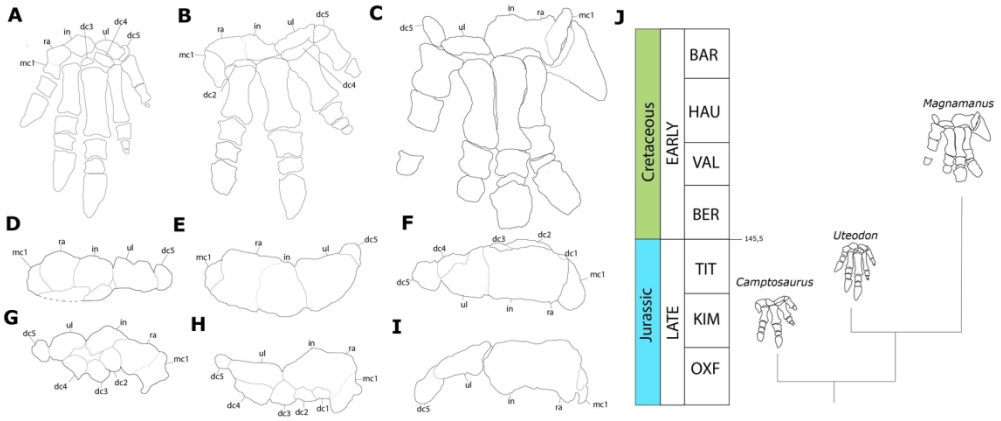

Fig.14. Comparative table of the manual anatomy of selected styracosternans. *Uteodon aphanoecetes* left manus (specimen CM 11337) in (A) extensor view, (D) proximal view and (G) palmar view. *Camptosaurus dispar* right manus, reversed (specimen USNM 4277) in (B) extensor view, (E) proximal view and (H) palmar view (holotype USNM 4282). *Magnamanus soriaensis* right manus (holotype MNS 2000) in (C) extensor view, (F) proximal view and (I) palmar view. Note the difference in the structure of the carpus: *Uteodon aphanoecetes* presents a partially fused and not closely packed carpus, *Camptosaurus dispar* presents a partially fused but closely packed carpus while *Magnamanus soriaensis* presents the typical stout and fused element of Styracosterna. (J) Stratigraphic distribution of these characters. Abbreviations: dc1: distal carpal 1, dc2: distal carpal 2, dc3: distal carpal 3, dc4: distal carpal4, dc5: distal carpal 5, in: intermedium, mc1: metacarpal 1, ra: radiale, ul: ulnare.

165x75mm (300 x 300 DPI)

Fig.15. Life restoration of Draconyx loureiroi, in the environment represented by Lourinhã Formation. Credit to Victor Carvalho, used with permission under CC BY NC license.

1357x652mm (72 x 72 DPI)